



1 **Heterogeneous reaction of ClONO₂ with TiO₂ and SiO₂ aerosol particles:**
2 **implications for stratospheric particle injection for climate engineering**

3 M. J. Tang^{1,2,7}, J. Keeble¹, P. J. Telford^{1,3}, F. D. Pope⁴, P. Braesicke⁵, P. T. Griffiths^{1,3}, N. L.

4 Abraham^{1,3}, J. McGregor⁶, I. M. Watson², R. A. Cox¹, J. A. Pyle^{1,3}, M. Kalberer^{1,*}

5

6 1 Department of Chemistry, University of Cambridge, Cambridge CB2 1EW, UK

7 2 School of Earth Sciences, University of Bristol, Bristol BS8 1RJ, UK

8 3 National Centre for Atmospheric Science, NCAS, UK

9 4 School of Geography, Earth and Environmental Sciences, University of Birmingham,
10 Birmingham B15 2TT, UK

11 5 IMK-ASF, Karlsruhe Institute of Technology, Karlsruhe, Germany

12 6 Department of Chemical and Biological Engineering, University of Sheffield, Sheffield S1

13 3JD, UK

14 7 State Key Laboratory of Organic Geochemistry, Guangzhou Institute of Geochemistry,
15 Chinese Academy of Sciences, Guangzhou 510640, China

16

17 Correspondence: M. Kalberer (markus.kalberer@atm.ch.cam.ac.uk)



18 Abstract

19 Deliberate injection of aerosol particles into the stratosphere is a potential climate
20 engineering scheme. Introduction of particles into the stratosphere would scatter solar radiation
21 back to space, thereby reducing the temperature at the Earth's surface and hence the impacts
22 of global warming. Minerals such as TiO_2 or SiO_2 are among the potentially suitable aerosol
23 materials for stratospheric particle injection due to their greater light scattering ability
24 compared to stratospheric sulfuric acid particles. However, the heterogeneous reactivity of
25 mineral particles towards trace gases important for stratospheric chemistry largely remains
26 unknown, precluding reliable assessment of their impacts on stratospheric ozone which is of
27 key environmental significance. In this work we have investigated for the first time the
28 heterogeneous hydrolysis of ClONO_2 on TiO_2 and SiO_2 aerosol particles at room temperature
29 and at different relative humidities (RH), using an aerosol flow tube. The uptake coefficient,
30 $\gamma(\text{ClONO}_2)$, on TiO_2 was $\sim 1.2 \times 10^{-3}$ at 7% and remaining unchanged at 33% RH, and increased
31 for SiO_2 from $\sim 2 \times 10^{-4}$ at 7% RH to $\sim 5 \times 10^{-4}$ at 35% RH, reaching a value of $\sim 6 \times 10^{-4}$ at 59%
32 RH. We have also examined the impacts of a hypothetical TiO_2 injection on stratospheric
33 chemistry using the UKCA chemistry-climate model in which heterogeneous hydrolysis of
34 N_2O_5 and ClONO_2 on TiO_2 particles is considered. A TiO_2 injection scenario with a solar
35 radiation scattering effect very similar to the eruption of Mt. Pinatubo was constructed. It is
36 found that compared to the eruption of Mt. Pinatubo, TiO_2 injection causes less ClOx activation
37 and less ozone destruction in the lowermost stratosphere, while reduced depletion of N_2O_5 and
38 NOx in the middle stratosphere results in decreased ozone levels. Overall, no significant
39 difference in the vertically integrated ozone abundancies is found between TiO_2 injection and
40 the eruption of Mt. Pinatubo. Future work required to further assess the impacts of TiO_2
41 injection on stratospheric chemistry is also discussed.



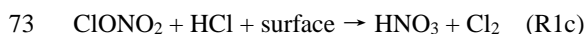
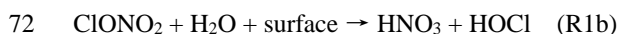
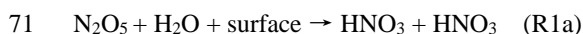
42 **1 Introduction**

43 Climate engineering (also known as geoengineering), the deliberate and large-scale
44 intervention in the Earth's climatic system to reduce global warming (Shepherd, 2009), has
45 been actively discussed by research communities and is also beginning to surface in the public
46 consciousness. The injection of aerosol particles (or their precursors) into the stratosphere to
47 scatter solar radiation back into space is one of the solar-radiation management (SRM) schemes
48 proposed for climate engineering (Crutzen, 2006). Sulfuric acid particles, due to their natural
49 presence in the stratosphere (SPARC, 2006), have been the main focus of stratospheric particle
50 injection research (Crutzen, 2006; Ferraro et al., 2011; Kravitz et al., 2013; Tilmes et al., 2015;
51 Jones et al., 2016). Very recently, minerals with refractive indices higher than sulphuric acid,
52 e.g., TiO₂ and SiO₂, have been proposed as possible alternative particles to be injected into the
53 stratosphere for climate engineering (Pope et al., 2012). For example, the refractive index at
54 550 nm is 2.5 for TiO₂ and 1.5 for stratospheric sulfuric acid particles. If the size of TiO₂
55 particles used for SRM can be optimized, it is estimated that compared to sulfuric acid particles,
56 the use of TiO₂ requires a factor of ~3 less in mass (and a factor of ~7 less in volume) in order
57 to achieve the same solar radiation scattering effect (Pope et al., 2012).

58 Injecting particles into the stratosphere would increase the amount of aerosol particles in
59 the stratosphere, thus increasing the surface area available for heterogeneous reactions (e.g.,
60 R1a, R1b, and R1c), whose effects on stratospheric chemistry and in particular on stratospheric
61 ozone depletion have been well documented for sulfuric acid particles (Molina et al., 1996;
62 Solomon, 1999). The background burden of sulfuric acid particles in the stratosphere, i.e.
63 during periods with low volcanic activities, is 0.65±0.2 Tg (SPARC, 2006). The eruption of
64 Mt. Pinatubo in 1991 delivered an additional ~30 Tg sulfuric acid particles into the stratosphere
65 (Guo et al., 2004) and subsequently produced record low levels of stratospheric ozone
66 (McCormick et al., 1995), in addition to causing substantial surface cooling (Dutton and



67 Christy, 1992). Observation and modelling studies have further suggested that, after the
68 eruption of Mt. Pinatubo, significant change in the partitioning of nitrogen and chlorine species
69 in the stratosphere occurred (Fahey et al., 1993; Wilson et al., 1993; Solomon, 1999), caused
70 by heterogeneous reactions of N_2O_5 and ClONO_2 (R1a-R1c):



74 Therefore, before any types of material can be considered for stratospheric particle injection,
75 their impact on stratospheric chemistry and ozone in particular has to be well understood
76 (Tilmes et al., 2008; Pope et al., 2012).

77 Heterogeneous reactions on sulfuric acid and polar stratospheric clouds (PSCs) have been
78 extensively studied and well characterized (Crowley et al., 2010; Ammann et al., 2013;
79 Burkholder et al., 2015). However, the reactivity of minerals (e.g., TiO_2 and SiO_2) towards
80 reactive trace gases in the stratosphere has received much less attention. For example, the
81 heterogeneous reactions of ClONO_2 with silica (SiO_2) and alumina (Al_2O_3) in the presence of
82 HCl (R1c) have only been explored by one previous study (Molina et al., 1997) in which
83 minerals coated on the inner wall of a flow tube were used. Further discussion of this work is
84 provided in Section 4.4. The lack of high quality kinetic data for important reactions impedes
85 reliable assessment of assessing the impact of injecting mineral particles into the stratosphere
86 on stratospheric ozone (Pope et al., 2012). TiO_2 is an active photo-catalyst and its atmospheric
87 heterogeneous photochemistry also therefore deserves further investigation (Shang et al., 2010;
88 Chen et al., 2012; Romanias et al., 2012; Kebede et al., 2013; George et al., 2015).

89 To address these issues, in our previous work we have investigated the heterogeneous
90 reactions of N_2O_5 with TiO_2 (Tang et al., 2014d) and SiO_2 (Tang et al., 2014a) particles (R1a).
91 That work is extended here to the investigation of the heterogeneous hydrolysis of ClONO_2 on



92 TiO₂ and SiO₂ (R1b) using an aerosol flow tube. There are only a few previous studies in which
93 the reactions of ClONO₂ with airborne particles or droplets have been examined. For example,
94 the interaction of ClONO₂ with sulfuric acid aerosol particles was investigated using aerosol
95 flow tubes (Hanson and Lovejoy, 1995; Ball et al., 1998; Hanson, 1998). Droplet train
96 techniques were used to study the heterogeneous reactions of ClONO₂ with aqueous droplets
97 containing sulfuric acid (Robinson et al., 1997) or halide (Deiber et al., 2004). The interaction
98 of ClONO₂ with airborne water ice particles was also examined (Lee et al., 1999). Our
99 experimental work, carried out at room temperature and at different RH, is the first study which
100 has investigated the heterogeneous interaction of ClONO₂ with airborne mineral particles. In
101 the lower stratosphere into which particles would be injected, typical temperature and RH
102 ranges are 200-220 K and <40%, respectively (Dee et al., 2011). We note that while our
103 experimental work covers the RH range relevant for the lower stratosphere, it has only been
104 performed at room temperature instead of 200-220 K due to experimental challenges.

105 ClONO₂ may also play a role in tropospheric chemistry (Finlayson-Pitts et al., 1989)
106 though its presence in the troposphere has not yet been confirmed by field measurements. The
107 importance of Cl atoms in tropospheric oxidation capacity has received increasing attention in
108 recent years (Simpson et al., 2015), and precursors of Cl atoms, e.g., ClNO₂ (Osthoff et al.,
109 2008; Thornton et al., 2010; Phillips et al., 2012; Bannan et al., 2015; Wang et al., 2016), Cl₂
110 (Spicer et al., 1998; Riedel et al., 2012; Liao et al., 2014), and HOCl (Lawler et al., 2011), have
111 been detected in the troposphere at various locations. Cl atoms react with O₃ to form ClO
112 radicals, which react with NO₂ to produce ClONO₂. The uptake of ClONO₂ by aerosol particles
113 (R1b, R1c) may recycle ClONO₂ to more photolabile species (HOCl or Cl₂) and thus amplify
114 the impact of Cl atoms on tropospheric oxidation capacity (Finlayson-Pitts et al., 1989; Deiber
115 et al., 2004). Considering the widespread occurrence of reactive chlorine species (Simpson et
116 al., 2015) and mineral dust particles (Textor et al., 2006; Ginoux et al., 2012; Tang et al., 2016)



117 in the troposphere, our laboratory measurements can also have strong implications for
118 tropospheric chemistry.

119 Using the UKCA (United Kingdom Chemistry and Aerosol model) chemistry-climate
120 model, a preliminary assessment of the effect of injecting TiO₂ into the stratosphere on
121 stratospheric chemistry and ozone was discussed in our previous work (Tang et al., 2014d).
122 This model was also used to investigate stratospheric ozone change due to volcanic sulfuric
123 acid particles after the eruption of Mt. Pinatubo in 1991 (Telford et al., 2009). In the previous
124 work (Tang et al., 2014d), we used the UKCA model to construct a case study in which TiO₂
125 aerosols were distributed in the stratosphere in a similar way to the volcanic sulfuric acid
126 particles after the eruption of Mt. Pinatubo so that the solar radiation scattering effect was
127 similar for the two scenarios; however, the only heterogeneous reaction on TiO₂ particles
128 considered was the uptake of N₂O₅ (R1a). Injection of solid aerosols into the stratosphere can
129 have a significant impact on ozone mixing ratios when heterogeneous reactions involving
130 chlorine are considered (Weisenstein et al., 2015). Several previous studies (Jackman et al.,
131 1998; Danilin et al., 2001; Weisenstein et al., 2015) have considered the effects of solid alumina
132 particles on stratospheric chemistry; however, there is only very limited assessment of other
133 potential solid aerosol compositions (e.g., TiO₂ and diamond) (Tang et al., 2014d). Here we
134 expand upon the previous literature by considering in our model a number of heterogeneous
135 reactions with new kinetic data on TiO₂. In our current work the heterogeneous hydrolysis of
136 ClONO₂ on TiO₂ particles (R1b) has been included, using our new experimental data. The
137 changes in stratospheric ozone and reactive nitrogen and chlorine species are assessed by
138 comparing to the impact of the Mt. Pinatubo eruption.

139 **2 Experimental section**

140 The heterogeneous reaction of ClONO₂ with aerosol particles was investigated at
141 different RH using an atmospheric pressure aerosol flow tube (AFT). In addition, its uptake



142 onto Pyrex glass was also studied, using a coated wall flow tube. N₂ was used as carrier gas,
143 and all the experiments were carried out at 296±2 K.

144 **2.1 Aerosol flow tube**

145 **2.1.1 Flow tube**

146 A detailed description of the AFT was given in our previous work (Tang et al., 2014a;
147 Tang et al., 2014d), and only the key features are described here. The flow tube, as shown in
148 Figure 1, is a horizontally-mounted Pyrex glass tube (i.d.: 3.0 cm; length: 100 cm). The total
149 flow in the AFT was 1500 mL/min, leading to a linear flow velocity of 3.54 cm s⁻¹ and a
150 maximum residence time of ~30 s. The Reynolds number is calculated to be 69, suggesting a
151 laminar flow condition in the flow tube. Under our experimental conditions, the entrance length
152 needed to develop the laminar flow is ~12 cm. The mixing length is calculated to be ~14 cm,
153 using a diffusion coefficient of 0.12 cm² s⁻¹ for ClONO₂ in N₂ at 296 K (Tang et al., 2014b).
154 Only the middle part of the flow tube (30-80 cm) was used to measure the uptake kinetics.

155 A commercial atomizer (Model 3076, TSI, USA) was used to generate an ensemble of
156 mineral aerosols. N₂ at ~3 bar was applied to the atomizer to disperse the mineral/water mixture
157 (with a TiO₂ or SiO₂ mass fraction of ~0.5%), resulting in an aerosol flow of 3000 mL/min.
158 The aerosol flow was delivered through two diffusion dryers, and the resulting RH was adjusted
159 by varying the amount of silica gel in the diffusion dryers. 1200 mL/min flow was pumped
160 away through F1, and the remaining flow (1800 mL/min) was then delivered through a cyclone
161 (TSI, USA) to remove super-micrometre particles. This cyclone has a cut-off size of 800 nm
162 at a flow rate of 1000 mL/min. The aerosol flow could be delivered through a filter to remove
163 all the particles (to measure the wall loss rate), or alternatively the filter could be bypassed to
164 introduce aerosol particles into the AFT (to measure the total loss rate). Beyond that point, 300
165 mL/min was sampled by a scanning mobility particle sizer (SMPS), and the remaining 1500
166 mL/min flow was delivered into the AFT via the side arm. Mineral aerosols were characterized



167 online using a SMPS, consisting of a differential mobility analyser (DMA, TSI 3081) and a
168 condensation particle counter (CPC, TSI 3775) which was operated with a sampling flow rate
169 of 300 mL/min. The sheath flow of the DMA was set to 2000 mL/min, giving a detectable
170 mobility size range of 19-882 nm. The time resolution of the SMPS measurement was 150 s.

171 The bottom 30 cm of the AFT was coaxially inserted into another Pyrex tube (inner
172 diameter: 4.3 cm; length: 60 cm). A sheath flow (F2, 1500 mL/min) was delivered through the
173 annular space between the two coaxial tubes. The sheath flow has the same linear velocity as
174 the aerosol flow to minimize the turbulence at the end of the aerosol flow tube where the two
175 flows joined. Gases could exchange between the sheath flow and the aerosol flow because of
176 their large diffusion coefficients ($\sim 0.1 \text{ cm}^2 \text{ s}^{-1}$) (Tang et al., 2014b), while aerosol particles
177 remained in the centre due to their much smaller diffusion coefficients, i.e. 10^{-7} - $10^{-6} \text{ cm}^2 \text{ s}^{-1}$
178 (Hinds, 1996). At the end of the large Pyrex tube, a flow of 500 mL/min was sampled through
179 a 1/4" FEP tube which intruded 1-2 mm into the flow close to the wall of the Pyrex tube. This
180 gas-particle separation method enabled particle-free gas to be sampled, despite very high
181 aerosol concentrations used in the AFT. Sampling particle-free gas prevents particles from
182 deposition onto the inner wall of the sampling tube, and therefore minimizes the undesired loss
183 of the reactive trace gases (e.g., ClONO₂ in this study) during their transport to the detector.
184 More detailed discussion of this gas-particle separation method used in the aerosol flow
185 experiments are provided elsewhere (Rouviere et al., 2010; Tang et al., 2012).

186 2.1.2 ClONO₂ synthesis

187 ClONO₂ was synthesized in the lab by reacting Cl₂O with N₂O₅ (Davidson et al., 1987;
188 Fernandez et al., 2005). N₂O₅ crystals were synthesized by trapping the product formed from
189 mixing NO with O₃ in large excess (Fahey et al., 1985). The synthesis and purification is
190 detailed in our previous study (Tang et al., 2014d). Cl₂O was synthesized by reacting HgO with
191 Cl₂ (Renard and Bolker, 1976; Molina et al., 1977). Cl₂ from a lecture bottle was first trapped



192 as yellow-green liquid (a few mL) in a glass vial at $-76\text{ }^{\circ}\text{C}$ using an ethanol-dry ice bath. It was
193 then warmed up to room temperature so that all the Cl_2 was evaporated and transferred to the
194 second glass vessel which contained HgO powders in excess and was kept at $-76\text{ }^{\circ}\text{C}$. The glass
195 vessel containing liquid Cl_2 and HgO powders was sealed and kept at $-76\text{ }^{\circ}\text{C}$ overnight. It was
196 then warmed up to room temperature to evaporate and transfer the formed Cl_2O and any
197 remaining Cl_2 to the third glass vial kept at $-76\text{ }^{\circ}\text{C}$. Liquid Cl_2O appeared dark reddish-brown
198 in colour.

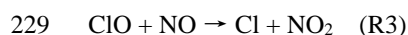
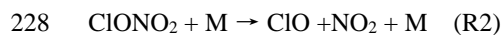
199 The third vessel containing Cl_2O was warmed up to room temperature to evaporate and
200 transfer Cl_2O to the fourth vial which contained synthesized N_2O_5 and was kept at $-76\text{ }^{\circ}\text{C}$. The
201 vial containing Cl_2O and N_2O_5 was sealed and kept at $-50\text{ }^{\circ}\text{C}$ for 2-3 days in a cryostat. In this
202 work Cl_2O was in slight excess compared to N_2O_5 , and thus all the white powder (solid N_2O_5)
203 was consumed. ClONO_2 is liquid at $-50\text{ }^{\circ}\text{C}$, with a colour similar to liquid Cl_2 . The major
204 impurity of our synthesized ClONO_2 was Cl_2O , and the boiling temperature at 760 Torr is $2\text{ }^{\circ}\text{C}$
205 for Cl_2O and $\sim 22\text{ }^{\circ}\text{C}$ for ClONO_2 (Stull, 1947; Renard and Bolker, 1976). To purify our
206 synthesized ClONO_2 , the vial containing ClONO_2 was warmed up to $5\text{ }^{\circ}\text{C}$ and connected to a
207 small dry N_2 flow via a T-piece for a few hours. Note that the N_2 flow was not delivered into
208 the vial but instead served a dry atmosphere at ~ 760 Torr. Cl_2O was boiled at $5\text{ }^{\circ}\text{C}$ and diffused
209 passively into the N_2 flow. Cl_2 was also removed because its boiling temperature is $-34\text{ }^{\circ}\text{C}$
210 (Stull, 1947). The amount of N_2O_5 in ClONO_2 was minimized because Cl_2O was in excess. In
211 addition, the vapour pressure (a few mTorr) of N_2O_5 (Stull, 1947) is >100 times lower than that
212 of ClONO_2 (~ 1 Torr) at around $-76\text{ }^{\circ}\text{C}$ (Schack and Lindahl, 1967; Ballard et al., 1988;
213 Anderson and Fahey, 1990); therefore, even if N_2O_5 was present in the gas phase, its amount
214 would be negligible compared to ClONO_2 .



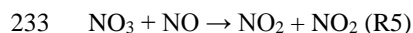
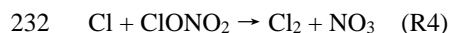
215 2.1.3 ClONO₂ detection

216 The ClONO₂ vial was stored at -76 °C in the dark using a cryostat. A small dry N₂ flow
217 (a few mL/min, F3) was delivered into the vial to elute gaseous ClONO₂. The ClONO₂ flow
218 was delivered through 1/8" FEP tubing in a stainless-steel injector into the centre of the aerosol
219 flow tube. The position of the injector could be adjusted to vary the interaction time of ClONO₂
220 with aerosols in the flow tube.

221 The flow sampled from the flow tube (500 mL/min) was mixed with ~5 mL/min NO (100
222 ppmv in N₂) and then delivered into a glass reactor heated to 130 °C. The initial NO mixing
223 ratio (in the absence of ClONO₂) in the reactor was ~1000 ppbv (or ~1.8×10¹³ molecule cm⁻³).
224 The volume of the glass reactor (inner diameter: 2.0 cm; length: 10 cm) is ~30 cm³,
225 corresponding to an average residence time of ~2.6 s at 130 °C. ClONO₂ was thermally
226 decomposed in the reactor to ClO and NO₂ (R2, where M is the third molecule, e.g., N₂), and
227 ClO was then titrated by NO in excess (R3):



230 Cl atoms produced in reaction (R3) further reacted with ClONO₂ (R4), and the NO₃ radicals
231 formed were titrated by NO (R5):



234 If the thermal dissociation of ClONO₂ (R2) and the scavenging of ClO and NO₃ radicals by
235 NO (R3, R4) all reach completion, the initial mixing ratio of ClONO₂ is equal to the decrease
236 in the NO mixing ratios before and after introducing ClONO₂ into the reactor (Anderson and
237 Fahey, 1990).

238 The lifetime of ClONO₂ with respect to thermal dissociation (R2) at 130 °C was estimated
239 to be ~0.2 s at 160 Torr (Anderson and Fahey, 1990), and further increase in pressure to ~760



240 Torr would increase the decomposition rate and reduce its lifetime. The lifetime of ClONO₂
241 with respect to reaction (R4) is not critical for our purpose although it enhances the overall
242 decay of ClONO₂ in the reactor. The second order rate constants are $1.3 \times 10^{-11} \text{ cm}^3 \text{ molecule}^{-1}$
243 s^{-1} for the reaction of ClO with NO and $2.3 \times 10^{-11} \text{ cm}^3 \text{ molecule}^{-1} \text{ s}^{-1}$ for the reaction of NO₃
244 with NO at 130 °C (Burkholder et al., 2015), giving lifetimes of $\sim 4 \times 10^{-3} \text{ s}$ for ClO with respect
245 to reaction (R3) and $\sim 2 \times 10^{-3} \text{ s}$ for NO₃ with respect to reaction (R5) in the presence of ~ 1000
246 ppbv NO in the reactor. To conclude, under our experimental conditions, the residence time of
247 the gas flow in the heated reactor was long enough for the completion of thermal dissociation
248 of ClONO₂ (R2) and titrations of ClO and NO₃ by NO (R3 and R5).

249 The flow exiting the reactor was sampled by a chemiluminescence-based NO_x analyser
250 (Model 200E, Teledyne Instruments, USA), which has a sampling flow rate of 500 mL/min
251 ($\pm 10\%$). This instrument has two modes. In the first mode NO is measured by detecting the
252 chemiluminescence of exited NO₂ (NO₂^{*}) produced by reacting NO with O₃ in excess. The gas
253 flow can also be passed through a convertor cartridge filled with molybdenum (Mo) chips
254 heated to 315 °C and all the NO₂ (and very likely also some of other NO_y, e.g., HONO, HNO₃)
255 is converted to NO; in this mode the total NO (initial NO and NO converted from NO₂ etc.) is
256 measured and termed as NO_x. The two modes are periodically switched, and the instrument
257 has a detection limit of 0.5 ppbv with a time resolution of 1 min.

258 The response of measured NO and NO_x mixing ratios to the introduction of ClONO₂ into
259 the AFT is displayed in Figure 2. Both the sheath flow and the flow in the AFT were set to
260 1500 mL/min (dry N₂), and the injector was at 40 cm. The introduction of ClONO₂ into the
261 AFT at ~ 20 min leads to the decrease of NO (solid curve in Figure 2a) from ~ 1100 ppbv to
262 ~ 400 ppbv, and NO recovered to its initial level after stopping the ClONO₂ flow at ~ 120 min.
263 The ClONO₂ mixing ratio (solid curve in Figure 2b), derived from the change in the NO mixing
264 ratio, was very stable over 100 min. As expected, the introduction of ClONO₂ into the system



265 led to the increase of the measured NO_x mixing ratio (dashed curve in Figure 2a). Ideally the
266 increase in NO_x mixing ratios due to the introduction of ClONO₂ should be equal to the
267 ClONO₂ mixing ratio. The nitrogen balance (dashed curve in Figure 2b), defined as the
268 difference in the ClONO₂ mixing ratios (equal to the change in NO mixing ratios) and the
269 change of the NO_x mixing ratios, is essentially zero within the experimental noise level. This
270 gives us further confidence in the purity of our synthesized ClONO₂: under our current
271 detection scheme the change in the NO_x mixing ratios will be twice of the N₂O₅ mixing ratio,
272 and therefore N₂O₅ contained in the ClONO₂ flow as an impurity was negligible. This method
273 provides a simple and relatively selective method to quantify ClONO₂, and could be used to
274 calibrate other ClONO₂ detection methods (Anderson and Fahey, 1990). One previous study
275 used a similar method to detect ClONO₂ in their experiments of ClONO₂ uptake onto sulfuric
276 acid aerosol particles (Ball et al., 1998), with the only difference being that in their study NO
277 was detected by its absorption at 1845.5135 cm⁻¹. Their reported $\gamma(\text{ClONO}_2)$ onto sulfuric acid
278 aerosol particles are in good agreement with those measured by other studies in which ClONO₂
279 was measured using mass spectroscopy. This suggests that the indirect detection method of
280 ClONO₂ utilized by Ball et al. (1998) and in this work can be used to investigate the uptake of
281 ClONO₂ onto aerosol particles.

282 2.2 Coated-wall flow tube

283 The coated-wall flow tube, a Pyrex glass tube with an inner diameter of 30 mm, was used
284 to measure the uptake of ClONO₂ onto fresh Pyrex glass. The inner wall was rinsed with diluted
285 NaOH solution and then by methanol and deionized water. A flow of 1500 mL/min, humidified
286 to the desired RH, was delivered into the top of the flow tube via a side arm. A small N₂ flow
287 was used to elute the liquid ClONO₂ sample, and the flow was then delivered through a 1/8''
288 Teflon tube in a stainless steel injector into the centre of the flow tube. The position of the
289 injector could be changed to vary the interaction time between ClONO₂ and the inner wall of



290 the flow tube. At the bottom of the flow tube, a flow of 500 mL/min was sampled through
291 another side arm, mixed with ~5 mL/min NO (100 ppmv in N₂), and then delivered into a glass
292 reactor heated to 130 °C. The flow exiting the heated glass reactor was then sampled into a
293 NO_x analyser. The method used to detect ClONO₂ is detailed in Section 2.1. The remaining
294 flow (~1000 mL/min) went through a RH sensor into the exhaust.

295 The linear flow velocity in the flow tube is 3.54 cm s⁻¹ with a Reynolds number of 69,
296 suggesting that the flow is laminar. The length of the flow tube, defined as the distance between
297 the side arm through which the main flow was delivered into the flow tube and the other side
298 arm through which 500 mL/min was sampled from the flow tube into the NO_x analyser, is 100
299 cm, giving a maximum residence time of ~30 s. The entrance length required to fully develop
300 the laminar flow and the mixing length required to fully mix ClONO₂ with the main flow are
301 both less than 15 cm. The loss of ClONO₂ onto the inner wall was measured using the middle
302 part (30-80 cm) of the flow tube.

303 2.3 Chemicals

304 NO (>99% purity) in a lecture bottle and the 100 ppmv (±1 ppmv) NO in N₂ were supplied
305 by CK Special Gas (UK). Pure Cl₂ (with a purity of >99.5%) in a lecture bottle and HgO
306 (yellow powder, with a purity of >99%) were provided by Sigma-Aldrich (UK). N₂ and O₂
307 were provided by BOC Industrial Gases (UK). P25 TiO₂, with an anatase to rutile ratio of 3:1,
308 was supplied by Degussa-Hüls AG (Germany). SiO₂ powders with a stated average particle
309 size (aggregate) of 200-300 nm were purchased from Sigma-Aldrich (UK). The BET surface
310 area is 8.3 m² g⁻¹ for TiO₂ (Tang et al., 2014d) and ~201 m² g⁻¹ for SiO₂ (Tang et al., 2014a).

311 3 Model description

312 The UKCA chemistry-climate model in its coupled stratosphere-troposphere
313 configuration, which combines both the tropospheric (O'Connor et al., 2014) and stratospheric
314 (Morgenstern et al., 2009) schemes, was used to simulate the effect of heterogeneous



315 hydrolysis of N_2O_5 (R1a) and ClONO_2 (R1b) on TiO_2 . In this model the chemical cycles of Ox,
316 HOx and NOx, the oxidation of CO, ethane, propane and isoprene, chlorine and bromine
317 chemistry, and heterogeneous reactions on sulfuric acid and polar stratospheric clouds are all
318 included. The same approach used to investigate the effects of the eruption of Mt. Pinatubo on
319 stratospheric ozone (Telford et al., 2009) is adopted in this study. Telford et al. (2009) used the
320 UKCA model in a “nudged” configuration by constraining the dynamics of the model to
321 observations (Telford et al., 2008), and evaluated the difference of stratospheric ozone with
322 and without the additional sulfuric acid aerosols caused by the eruption of Mt. Pinatubo.

323 In our current study three simulations are used to assess the effects of TiO_2 particle
324 injection into the stratosphere. All three simulations are started from a spun-up initial condition
325 and run from December 1990 to January 1993. In the base scenario (S1), an aerosol climatology
326 is used which represents the background loading of stratospheric sulphate aerosol. Alongside
327 S1 two further simulations were performed, one representing the eruption of Mt. Pinatubo in
328 June 1991 (S2) and a second (S3) in which the Mt. Pinatubo eruption is replaced with a single
329 injection of TiO_2 particles on the same date. The simulations are set up so that the radiative
330 impacts at the surface are comparable between S2 and S3. Pope et al. (2012) have proposed
331 that 10 Tg of TiO_2 aerosol particles with an assumed radius of 70 nm are required in order to
332 achieve the same solar radiation scattering effect as the eruption of Mt. Pinatubo. The total
333 surface area of TiO_2 is calculated from the mass of TiO_2 particles, using a density of 4.23 g
334 cm^{-3} and an assumed radius of 70 nm, and the global distribution of TiO_2 is scaled to the sulfuric
335 acid aerosol distribution resulting from the eruption of Mt. Pinatubo. The sulfuric acid aerosol
336 surface area distribution was derived from the SPARC climatology (SPARC, 2006).

337 By running these three scenarios we are able to compare the relative impact of
338 stratospheric particle injection using TiO_2 compared to sulphate. The benefit of using the Mt.
339 Pinatubo eruption as the sulphate injection scenario is that it provides a natural analogue to



340 proposed climate engineering schemes, and the chemical and dynamical effects of the eruption
341 have been well documented. Telford et al. (2009) have shown that UKCA accurately models
342 the chemical impacts of the Mt. Pinatubo eruption, and the ozone bias is smaller now compared
343 to Telford et al. (2009).

344 It should be noted that all simulations are nudged to the same observed meteorological
345 conditions, following Telford et al. (2008). In this way we do not take into account the
346 radiative/dynamical feedbacks from any ozone changes resulting from chemical reactions
347 occurring on stratospheric aerosols, allowing just the chemical effects of stratospheric particle
348 injection to be quantified. The results presented here expand on our previous study (Tang et al.,
349 2014d) by including heterogeneous hydrolysis of both N_2O_5 (R1a) and ClONO_2 (R1b) on TiO_2 .
350 An uptake coefficient of 1.5×10^{-3} is used for R1a (reaction with N_2O_5) on TiO_2 particles as
351 determined by our previous measurement (Tang et al., 2014d). An uptake coefficient of
352 1.5×10^{-3} is used for R1b (heterogeneous hydrolysis of ClONO_2), which is slightly larger than
353 the experimental value measured in our current work (i.e. $\sim 1.2 \times 10^{-3}$ as shown in Section 4) and
354 represents an upper limit to the measured value given the experimental uncertainty. We use
355 this value to determine the maximum impact TiO_2 injection would have on stratospheric
356 chemistry.

357 **4 Results & Discussion**

358 **4.1 Uptake of ClONO_2 onto Pyrex glass**

359 The uptake of ClONO_2 onto fresh Pyrex glass wall was determined by measuring the
360 ClONO_2 concentrations at five different injection positions. The loss of ClONO_2 in the coated-
361 wall flow tube, under the assumption of pseudo first order kinetics, can be described by the Eq.
362 (1):

$$363 \quad [\text{ClONO}_2]_t = [\text{ClONO}_2]_0 \cdot \exp(-k_w \cdot t) \quad (1)$$



364 where $[\text{ClONO}_2]_t$ and $[\text{ClONO}_2]_0$ are the measured ClONO_2 concentrations at the reaction time
365 of t and 0, respectively, and k_w is the wall loss rate (s^{-1}). Two typical datasets of measured
366 $[\text{ClONO}_2]$ at five different injector positions are displayed in Figure 3, suggesting that ClONO_2
367 indeed follows the exponential decays, and the slopes of the exponential decays are equal to
368 k_w . The effective (or experimental) uptake coefficient of ClONO_2 , γ_{eff} , onto the Pyrex wall, can
369 then be calculated from k_w , using Eq. (2) (Howard, 1979; Wagner et al., 2008):

$$370 \quad \gamma_{\text{eff}} = \frac{k_w \cdot d_{\text{tube}}}{c(\text{ClONO}_2)} \quad (2)$$

371 where d_{tube} is the inner diameter of the flow tube (3.0 cm) and $c(\text{ClONO}_2)$ is the average
372 molecular speed of ClONO_2 ($25\,360 \text{ cm s}^{-1}$). Depletion of ClONO_2 close to the wall is caused
373 by the uptake of ClONO_2 onto the wall, and thus the effective uptake coefficient is smaller than
374 the true one. This effect can be corrected (Tang et al., 2014b), and the true uptake coefficients,
375 γ , are reported in Table 1.

376 The uptake coefficients of ClONO_2 onto Pyrex glass, as summarized in Table 1, increases
377 from $\sim 5 \times 10^{-6}$ at 0% RH to $\sim 1.6 \times 10^{-5}$ at 24% RH by a factor of ~ 3 . Uptake coefficients at higher
378 RH were not determined because the uptake coefficients determined at 24% RH ($\sim 1.6 \times 10^{-5}$)
379 are very close to the upper limit ($\sim 2.3 \times 10^{-5}$) which can be measured in this study using the
380 coated-wall flow tube technique due to the gas phase diffusion limit. The RH dependence of
381 $\gamma(\text{ClONO}_2)$ for Pyrex glass is further discussed in Section 4.4 together with these reported by
382 Molina et al. (1997) and our measurements on SiO_2 and TiO_2 aerosol particles.

383 **4.2 Reaction of ClONO_2 with SiO_2 and TiO_2 particles**

384 The uptake of ClONO_2 onto airborne SiO_2 and TiO_2 particles were investigated using an
385 atmospheric pressure aerosol flow tube, in which reactions with the aerosol particles and the
386 wall both contribute to the loss of ClONO_2 , as shown in Eq. (3):

$$387 \quad [\text{ClONO}_2]_t = [\text{ClONO}_2]_0 \cdot \exp[-(k_w + k_a) \cdot t] \quad (3)$$



388 where $[\text{ClONO}_2]_t$ and $[\text{ClONO}_2]_0$ are the measured ClONO_2 mixing ratios at the reaction times
389 of t and 0 s, and k_w and k_a are the loss rates (s^{-1}) of ClONO_2 onto the inner wall of the flow tube
390 and the surface of aerosol particles, respectively. In a typical uptake measurement, the aerosol
391 flow was delivered through a filter, and $[\text{ClONO}_2]$ was measured at five different injector
392 positions to determine the wall loss rate (k_w). The filter was then bypassed to deliver aerosol
393 particles into the flow tube, and the total ClONO_2 loss rate ($k_w + k_a$) in the flow tube was
394 determined. After that, the aerosol flow was passed through the filter to measure k_w again. The
395 variation of k_w determined before and after introducing particles into the flow tube was within
396 the experimental uncertainty of k_w , ensuring that the reactivity of the wall towards ClONO_2
397 remained constant during the uptake measurement.

398 The difference between the ClONO_2 loss rates without and with aerosol particles in the
399 flow tube, is equal to the loss rate due to the reaction with surface of aerosol particle (k_a). The
400 effective uptake coefficient of ClONO_2 onto aerosol particles, γ_{eff} , is related to k_a by Eq. (4)
401 (Crowley et al., 2010):

$$402 \quad k_a = 0.25 \cdot \gamma_{\text{eff}} \cdot c(\text{ClONO}_2) \cdot S_a \quad (4)$$

403 where S_a is the aerosol surface area concentration which can be derived from size-resolved
404 number concentrations (as shown in Figure S1) measured by the SMPS. Uptake of ClONO_2
405 onto aerosol particles also leads to the depletion of ClONO_2 near the particle surface and so the
406 effective uptake coefficient is smaller than the true uptake coefficient. This effect, which can
407 be corrected using the method described elsewhere (Tang et al., 2014b), is only a few percent
408 in this study as the particle diameters are $<1 \mu\text{m}$ and the uptake coefficient is relatively small
409 ($\sim 1 \times 10^{-3}$).

410 Two typical decays of ClONO_2 in the aerosol flow tube without and with $\text{SiO}_2/\text{TiO}_2$
411 aerosol particles in the flow tube are shown in Figure 4. For a majority of experiments, efforts
412 were made to generate enough aerosol particles so that k_a+k_w was significantly different to k_w .



413 It is evident from Figure 4 that the loss of ClONO₂ is significantly faster with TiO₂/SiO₂
414 particles in the flow tube than without aerosols. We acknowledge that the measured k_a and
415 therefore our reported γ in this study have quite large uncertainties. This is because the uptake
416 coefficients of ClONO₂ are very small and the surface area of the wall is ~1000 larger than that
417 of aerosol particles. This is the first time that heterogeneous reactions of ClONO₂ with airborne
418 mineral particles have been investigated.

419 The uptake coefficients of ClONO₂ are $\sim 1.2 \times 10^{-3}$ for TiO₂ particles, and no difference in
420 $\gamma(\text{ClONO}_2)$ at two different RH (7% and 33%) is found. The heterogeneous reaction of ClONO₂
421 with SiO₂ particles were studied at four different RH, with $\gamma(\text{ClONO}_2)$ increasing from $\sim 2 \times 10^{-4}$
422 at 7% RH to $\sim 5 \times 10^{-4}$ at 35% RH, reaching a value of $\sim 6 \times 10^{-4}$ at 59% RH. The uptake
423 coefficients of ClONO₂ are summarized in Table 2 for SiO₂ and TiO₂ aerosol particles, together
424 with key experimental conditions. In a few measurements in which the SiO₂ aerosol
425 concentrations were relatively low, the total ClONO₂ loss rate ($k_w + k_a$) was not different from
426 its wall loss rate (k_w) within the experimental uncertainty. In this case, only the upper limit of
427 k_a (and thus γ) can be estimated, which is reported here as the standard deviation of k_w . The
428 first three of the four uptake coefficients at $(17 \pm 2)\%$ RH for SiO₂ aerosol particles, tabulated
429 in Table 2, fall into this category. $\gamma(\text{ClONO}_2)$ on SiO₂ aerosol particles is around two orders of
430 magnitude larger than that on Pyrex glass. One explanation for such a large difference is that
431 SiO₂ particles used in our work are porous (Tang et al., 2014a) and therefore the surface area
432 which is actually available for the ClONO₂ uptake is much larger than that calculated using the
433 mobility diameters. In our previous study (Tang et al., 2014a) we have found that for SiO₂
434 particles, $\gamma(\text{N}_2\text{O}_5)$ calculated using the mobility diameter based surface area are a factor of 40
435 larger than those calculated using the BET surface area. Another reason is that the composition
436 of SiO₂ is different from Pyrex.



437 4.3 Effects of RH

438 The RH dependence of $\gamma(\text{ClONO}_2)$ for Pyrex glass is plotted in Figure 5 and exhibits a
439 positive dependence on RH, with $\gamma(\text{ClONO}_2)$ increased by a factor of ~ 3 when RH increases
440 from 0% to 24%. Previous studies (Hanson and Ravishankara, 1991; Hanson and Ravishankara,
441 1994; Zhang et al., 1994; Hanson, 1998) have shown that $\gamma(\text{ClONO}_2)$ for aqueous H_2SO_4
442 solution strongly depends on water content in the solution and it decreases from ~ 0.1 for 40%
443 H_2SO_4 to $\sim 1 \times 10^{-4}$ for 75% H_2SO_4 at 200-200 K, by a factor of ~ 1000 . It is suggested that the
444 heterogeneous uptake of ClONO_2 by aqueous H_2SO_4 solution proceeds via direct and acid-
445 catalysed hydrolysis (Robinson et al., 1997; Shi et al., 2001; Ammann et al., 2013). One may
446 expect that $\gamma(\text{ClONO}_2)$ for Pyrex glass will increase with RH. This is also supported by the
447 water adsorption isotherm on Pyrex glass particles (Chikazawa et al., 1984), showing that the
448 amount of adsorbed water on Pyrex surface displays a substantial increase at 20% RH
449 compared to that at 0% RH. However, the results reported by Chikazawa et al. (1984) are
450 presented graphically and thus impede us from a more quantitative discussion on the effect of
451 RH and surface-adsorbed water on uptake of ClONO_2 by Pyrex surface.

452 One can then expect that $\gamma(\text{ClONO}_2)$ may also increase with RH for the reaction with
453 SiO_2 and TiO_2 aerosol particles, since the amount of water adsorbed on these two types of
454 particles also increase with RH (Goodman et al., 2001). Inspection of the data listed in Table 2
455 reveals that $\gamma(\text{ClONO}_2)$ for SiO_2 particle increases from $\sim 2 \times 10^{-4}$ at 7% RH to $\sim 6 \times 10^{-4}$ at 59%
456 RH, and this is consistent with the large increase of adsorbed water on SiO_2 surface, from
457 around half a monolayer at $\sim 7\%$ RH to two monolayers at 60% RH (Goodman et al., 2001), as
458 shown in Figure S2. The uptake coefficients of ClONO_2 were measured to be $\sim 1.2 \times 10^{-3}$ for
459 TiO_2 at 7% and 33% RH, with no significant difference found at these two different RH. We
460 expect that further increase in RH will lead to larger $\gamma(\text{ClONO}_2)$ for TiO_2 , and future studies at
461 higher RH are needed to better understand the RH effects.



462 At similar RH (7% and 33%), $\gamma(\text{ClONO}_2)$ for TiO_2 are significantly larger than those for
463 SiO_2 . This may be explained by the larger amount of adsorbed water on TiO_2 at low and
464 medium RH compared to SiO_2 as shown in Figure S2. It is interesting to note that the uptake
465 of N_2O_5 shows different behaviour, i.e. $\gamma(\text{N}_2\text{O}_5)$ for SiO_2 (Tang et al., 2014a) are significantly
466 larger than that for TiO_2 at similar RH. This indicates that a different mechanism controls N_2O_5
467 uptake by mineral surfaces (Seisel et al., 2005; Tang et al., 2014a; Tang et al., 2014c): at low
468 RH the reaction with surface OH groups is the major pathway for the uptake of N_2O_5 onto
469 $\text{SiO}_2/\text{TiO}_2$ surface, instead of direct hydrolysis by surface-adsorbed water.

470 **4.4 Comparison with previous work**

471 We find that in the absence of HCl, $\gamma(\text{ClONO}_2)$ is around 1.2×10^{-3} for TiO_2 aerosol
472 particles and $< 1 \times 10^{-3}$ for SiO_2 aerosol particles at room temperature. Using the coated-wall
473 flow tube technique, Molina et al. (1997) investigated the uptake of ClONO_2 onto the inner
474 wall of an Al_2O_3 tube, $\alpha\text{-Al}_2\text{O}_3$ particles, and the inner wall of a Pyrex glass tube, in the
475 presence of $(1-10) \times 10^{-6}$ Torr HCl at 200-220 K. Uptake coefficients of ~ 0.02 were reported for
476 all the three types of surface (including Pyrex glass), over a factor of 1000 larger than
477 $\gamma(\text{ClONO}_2)$ for Pyrex glass determined in our present work. The large difference in $\gamma(\text{ClONO}_2)$
478 reported by the two studies is likely due to the co-presence of HCl (1×10^{-6} - 1×10^{-5} Torr) in the
479 experiments of Molina et al. (1997), while no HCl was present in our work. Heterogeneous
480 reactions of ClONO_2 proceed via direct and acid-catalysed hydrolysis (Robinson et al., 1997;
481 Shi et al., 2001; Ammann et al., 2013), and numerous previous studies have confirmed that the
482 presence of HCl in the gas phase (and thus partitioning into or adsorption onto the condensed
483 phases) promotes the uptake of ClONO_2 by H_2SO_4 solution, ice, and nitric acid trihydrate
484 (NAT), as summarized by Crowley et al. (2010), Sander et al. (2011) and Ammann et al. (2013).
485 Temperature may also play a role since measurements were carried out at 200-220 K by Molina
486 et al. (1997) and at ~ 296 K in our study.



487 Considering the importance of HCl in the ClONO₂ uptake and its abundance in the
488 stratosphere, it will be important to systematically measure $\gamma(\text{ClONO}_2)$ for SiO₂/TiO₂ in the
489 presence of HCl over a broad HCl concentration and temperature range relevant for lower
490 stratosphere.

491 **5 Implication for stratospheric particle injection**

492 Injection of TiO₂ into the stratosphere will provide additional surface area for the
493 heterogeneous reactions of N₂O₅ (R1a) and ClONO₂ (R1b, R1c). There are several important
494 types of particles naturally present in the stratosphere (Solomon et al., 1999), including sulfuric
495 acid, ice, and nitric acid trihydrate (NAT), and their interaction with ClONO₂ has been well
496 characterised (Crowley et al., 2010; Ammann et al., 2013; Burkholder et al., 2015). Comparing
497 $\gamma(\text{ClONO}_2)$ for TiO₂ particles with these other stratospherically relevant surfaces can provide
498 a first order estimate of their relative importance.

499 The uptake of ClONO₂ on H₂SO₄ acid particles is strongly influenced by temperature and
500 the water content in the particles (Shi et al., 2001; Ammann et al., 2013; Burkholder et al.,
501 2015): $\gamma(\text{ClONO}_2)$ are $<2 \times 10^{-3}$ for 65wt% H₂SO₄ particles and $<2 \times 10^{-4}$ for 75wt% H₂SO₄
502 particles. The global distribution of $\gamma(\text{ClONO}_2)$ calculated for sulfuric acid particles in the
503 stratosphere is shown in the supporting information (Figure S3), suggesting that $\gamma(\text{ClONO}_2)$ is
504 lower on TiO₂ particles than on sulfuric acid particles in the lower stratosphere. The uptake
505 coefficient of ClONO₂ for water ice shows a negative dependence on temperature, with
506 $\gamma(\text{ClONO}_2)$ of ~0.1 at ~200 K (Crowley et al., 2010; Burkholder et al., 2015), around a factor
507 of 100 larger than that for TiO₂ particles at room temperature. $\gamma(\text{ClONO}_2)$ for water-rich nitric
508 acid trihydrate (NAT), another important component for polar stratospheric clouds, increases
509 strongly with temperature, with $\gamma(\text{ClONO}_2)$ of 3.0×10^{-3} at 200 K, 6.0×10^{-3} at 210 K, and
510 1.14×10^{-2} at 220 K (Crowley et al., 2010).



511 While the background burden of stratospheric aerosol is low, volcanic eruptions and
512 deliberate stratospheric particle injection for climate engineering purposes have the potential
513 to significantly increase the available surfaces for heterogeneous reactions. In our current work,
514 three simulations were performed, one representing a low background loading of stratospheric
515 sulphate (<1 Tg) aerosols (S1), a second representing the eruption of Mt. Pinatubo (S2) and a
516 third representing an instantaneous injection of 10 Tg of TiO_2 (S3). SiO_2 particle injection is
517 not considered in our modelling study because the refractive index of SiO_2 is significantly
518 smaller than TiO_2 (Pope et al., 2012). Two heterogeneous reactions on TiO_2 particles, i.e.
519 heterogeneous hydrolysis of N_2O_5 (R1a) and ClONO_2 (R1b), were included in the simulation:
520 a value of 1.5×10^{-3} was used for $\gamma(\text{N}_2\text{O}_5)$, as measured in our previous work (Tang et al., 2014d),
521 and $\gamma(\text{ClONO}_2)$ was also set to 1.5×10^{-3} , based on the measurement reported in our current
522 study. All three simulations were nudged to observed meteorology from December 1990 to
523 January 1993. By comparing the TiO_2 injection (S3) with the Mt. Pinatubo eruption (S2) we
524 are able to quantify the relative impacts of TiO_2 and sulphuric acid injection on stratospheric
525 chemistry. Results in this section are presented as annual means for the year 1992.

526 Similar to our previous study (Tang et al., 2014d), we have found that injection of TiO_2
527 (S3) has a much reduced impact on stratospheric N_2O_5 concentrations than the eruption of Mt.
528 Pinatubo (S2). N_2O_5 mixing ratios are significantly reduced in S2 compared to S1 from 10-30
529 km, with concentrations reduced by $>80\%$ throughout most of this region. For comparison,
530 after TiO_2 injection (S3) N_2O_5 concentrations are reduced over a much smaller altitude range
531 (15-25 km) and to a lesser degree, with $\sim 20\%$ reductions in the tropics and up to 60% reductions
532 in the high latitudes. The relative effects of TiO_2 injection compared to sulphate injection on
533 N_2O_5 mixing ratios is calculated as the difference between S3 and S2. As shown in Figure 6,
534 throughout most of the stratosphere N_2O_5 mixing ratios remain higher under S3 than S2.



535 Under both particle injection scenarios (S2 and S3), stratospheric ClOx mixing ratios are
536 increased compared to S1 due to the activation of ClONO₂ through heterogeneous reactions.
537 However, Figure 7 suggests that ClOx mixing ratios are up to 40% lower in the tropical lower
538 stratosphere following the injection of TiO₂ aerosols compared to sulphate. This is driven in
539 part by the lower surface area density of TiO₂ compared to sulphate, but also due to the
540 difference in uptake coefficients. The uptake coefficient of ClONO₂ onto sulphate is
541 temperature dependent, and our measurements suggest that the uptake coefficient onto TiO₂ is
542 smaller than that for sulphate below ~215 K. Throughout much of the tropical lower
543 stratosphere where maximum aerosol surface area density is found in both S2 and S3,
544 temperatures are below ~220 K and therefore the uptake coefficient is lower for TiO₂ than
545 sulphate (as shown by Figure S3 in the supporting information), leading to reduced chlorine
546 activation. Previous studies have investigated the influence of temperature on the
547 heterogeneous reactions of mineral particles with a few other trace gases, including HCOOH
548 (Wu et al., 2012), H₂O₂ (Romanias et al., 2012) and OH radicals (Bedjanian et al., 2013), and
549 found that the measured uptake coefficients varied only by a factor of 2-3 or less across a wide
550 temperature range. Therefore, the temperature effect is not expected to be very significant in
551 our current work, although further studies are required to quantify and reduce these
552 uncertainties.

553 The relative difference in ozone mixing ratios following TiO₂ injection (S3) compared
554 with the eruption of Mt. Pinatubo (S2) is shown in Figure 8. Ozone mixing ratios in the lower
555 stratosphere decrease as a result of both TiO₂ and sulphate injection, with largest decreases
556 seen at high latitudes. In terms of annual means, the magnitude of this ozone response is
557 comparable between the two simulations, with a maximum of ~3% in the tropics and ~7% at
558 high latitudes. In contrast, ozone mixing ratios at the altitude of 25 km increase following the
559 eruption of Mt. Pinatubo (S2), but show no significant change upon TiO₂ injection (S3). This



560 is consistent with the much faster uptake of N_2O_5 onto sulphate aerosols and the resultant
561 stratospheric NO_x loss and decreases in the rates of catalytic ozone destruction at these altitudes.

562 The results presented here indicate that there is little difference in stratospheric ozone
563 concentrations between injection of TiO_2 and sulphate aerosols when R1a and R1b are
564 considered on TiO_2 . While TiO_2 injection (S3) leads to less ClO_x activation and ozone
565 destruction in the lowermost stratosphere, the reduced depletion of N_2O_5 and NO_x in the middle
566 stratosphere leads to decreased ozone mixing ratios compared to sulphate injection (S2). The
567 total column ozone differences between S3 and S2 are within $\pm 2.5\%$, indicating that there is
568 no significant difference in vertically integrated ozone abundancies and solar UV amounts
569 reaching the surface. However, more work is required to establish additional kinetic data for
570 heterogeneous reactions of TiO_2 .

571 **6 Conclusion**

572 Minerals with high refractive indices, such as TiO_2 , have been proposed as possible
573 materials used for stratospheric particle injection for climate engineering (Pope et al., 2012).
574 However, kinetic data of their heterogeneous reactions with important reactive trace gases (e.g.,
575 N_2O_5 and ClONO_2) in the stratosphere are lacking, impeding us from a reliable assessment of
576 the impacts of mineral particle injection on stratospheric ozone in particular and stratosphere
577 chemistry in general. In our current work, using an atmospheric pressure aerosol flow tube, we
578 have investigated the heterogeneous reaction of ClONO_2 with TiO_2 and SiO_2 aerosol particles
579 at room temperature and at different RH. The uptake coefficient, $\gamma(\text{ClONO}_2)$, was $\sim 1.2 \times 10^{-3}$ at
580 7% and 33% RH for TiO_2 particles, with no significant difference observed at these two RH;
581 for SiO_2 particles, $\gamma(\text{ClONO}_2)$ increases from $\sim 2 \times 10^{-4}$ at 7% RH to $\sim 6 \times 10^{-4}$ at 59%, showing a
582 positive dependence on RH. Therefore, it can be concluded that under similar conditions for
583 the RH range covered in this work, TiO_2 shows higher heterogeneous reactivity than SiO_2
584 towards ClONO_2 . Compared to sulfuric acid particles in the lower stratosphere, the



585 heterogeneous reactivity towards ClONO₂ is lower for TiO₂ particles. In addition, the
586 heterogeneous uptake of ClONO₂ by Pyrex glass was also studied, with $\gamma(\text{ClONO}_2)$ increasing
587 from $\sim 4.5 \times 10^{-6}$ at 0% RH to $\sim 1.6 \times 10^{-5}$ at 24% RH.

588 Using the UKCA chemistry-climate model with nudged meteorology, we have
589 constructed a scenario to assess the impact of TiO₂ particle injection on stratospheric chemistry.
590 In this scenario TiO₂ aerosol particles are distributed in the stratosphere in such a way that TiO₂
591 particle injection is assumed to produce a radiative effect similar to that of Mt. Pinatubo
592 eruption, following Pope et al. (2012). Heterogeneous reactions of N₂O₅ and ClONO₂ with
593 TiO₂ aerosol particles, both with an uptake coefficient of 1.5×10^{-3} based on our previous (Tang
594 et al., 2014d) and current laboratory experiments, were included in the simulation. It is found
595 that compared to the eruption of Mt. Pinatubo, the TiO₂ injection has a much smaller impact
596 on N₂O₅ in the stratosphere, although significant reduction (20-60% compared to the
597 background scenario without additional particle injection) in stratospheric N₂O₅ also occurs.
598 Compared to the background scenario, both TiO₂ injection and the Mt. Pinatubo eruption
599 scenarios lead to increased stratospheric ClOx mixing ratios, and the ClOx mixing ratios are
600 lower for the TiO₂ injection than the Mt. Pinatubo eruption. Both TiO₂ injection and the Mt.
601 Pinatubo eruption results in significant ozone depletion in the lower stratosphere, with largest
602 decreases occurring at high latitudes. In comparison with Mt. Pinatubo eruption, TiO₂ injection
603 causes less ClOx activation and less ozone destruction in the lowermost stratosphere, while the
604 reduced depletion of N₂O₅ and NOx in the middle stratosphere results in decreased ozone levels.
605 Overall, our simulation results suggest that there is no significant difference (within $\pm 2.5\%$) in
606 the vertically integrated ozone abundancies between TiO₂ injection and Mt. Pinatubo eruption.

607 It should be emphasized that heterogeneous chemistry of TiO₂ included in our current
608 modelling study is not complete. One example is the heterogeneous reaction of ClONO₂ with
609 HCl (R1c) on/in the particles. An uptake coefficient of 0.02 was reported for the heterogeneous



610 reaction of ClONO₂ with HCl on Al₂O₃ particles (Molina et al., 1997), and it is reasonable to
611 assume that this reaction may also be quite fast on TiO₂ particles. The heterogeneous reaction
612 of ClONO₂ with HCl on TiO₂ particles, with an uptake coefficient assumed to be the same as
613 that on Al₂O₃ surface (i.e. 0.02) as reported by Molina et al. (1997), has been included in further
614 simulations, and the results will be reported and discussed in a following paper. Other reactions,
615 including the heterogeneous reaction of HOCl (Molina et al., 1996; Solomon, 1999) and a range
616 of heterogeneous photochemical reactions (Chen et al., 2012; George et al., 2015), may also be
617 important and thus deserve further laboratory and modeling investigation.

618 Our nudged modeling simulations, designed to focus on chemistry effects, do not take
619 into account feedbacks between radiative effects, atmospheric dynamics, and chemistry.
620 Several recent studies have assessed the impact of high latitude stratospheric ozone depletion
621 using the UKCA model (Braesicke et al., 2013; Keeble et al., 2014) and have shown that
622 interactive feedbacks can affect stratospheric temperatures, the strength of the Brewer-Dobson
623 circulation, the longevity of polar vortices and surface climate. By nudging the model to
624 observed meteorology during the Mt. Pinatubo eruption these feedbacks are implicitly included
625 in the sulphate injection scenario. However, while we have chosen a TiO₂ loading to give the
626 same surface radiative response as the Mt. Pinatubo eruption, the stratospheric radiative
627 impacts may differ. In order to fully understand the true impact of stratospheric particle
628 injection, both the radiative and chemical effects, and the coupling between these responses,
629 need to be explored further. In addition, before any climate engineering schemes could be
630 considered, much consideration is absolutely obligatory, including, but not limited to, technical,
631 socioeconomic, political, environmental, and ethical feasibilities.

632 **Acknowledgement**

633 Financial support provided by EPSRC Grant EP/I01473X/1 and the Isaac Newton Trust
634 (Trinity College, University of Cambridge, U.K.) is acknowledged. We thank NCAS-CMS for



635 modelling support. Model integrations have been performed using the ARCHER UK National
636 Supercomputing Service. We acknowledge the ERC for support through the ACCI project
637 (project number: 267760).

638 **Reference**

- 639 Ammann, M., Cox, R. A., Crowley, J. N., Jenkin, M. E., Mellouki, A., Rossi, M. J., Troe, J.,
640 and Wallington, T. J.: Evaluated kinetic and photochemical data for atmospheric chemistry:
641 Volume VI - heterogeneous reactions with liquid substrates, *Atmos. Chem. Phys.*, 12, 8045-
642 8228, 2013.
- 643 Anderson, L. C., and Fahey, D. W.: Studies with ClONO₂: Thermal-dissociation rate and
644 catalytic conversion to NO using an NO/O₃ chemi-luminescence detector, *J. Phys. Chem.*, 94,
645 644-652, 1990.
- 646 Ball, S. M., Fried, A., Henry, B. E., and Mozurkewich, M.: The hydrolysis of ClONO₂ on
647 sub-micron liquid sulfuric acid aerosol, *Geophys. Res. Lett.*, 25, 3339-3342, 1998.
- 648 Ballard, J., Johnston, W. B., Gunson, M. R., and Wassell, P. T.: Absolute absorption
649 coefficients of ClONO₂ infrared bands at stratospheric temperatures, *J. Geophys. Res.-*
650 *Atmos.*, 93, 1659-1665, 1988.
- 651 Bannan, T. J., Booth, A. M., Bacak, A., Muller, J. B. A., Leather, K. E., Le Breton, M., Jones,
652 B., Young, D., Coe, H., Allan, J., Visser, S., Slowik, J. G., Furger, M., Prévôt, A. S. H., Lee,
653 J., Dunmore, R. E., Hopkins, J. R., Hamilton, J. F., Lewis, A. C., Whalley, L. K., Sharp, T.,
654 Stone, D., Heard, D. E., Fleming, Z. L., Leigh, R., Shallcross, D. E., and Percival, C. J.: The
655 first UK measurements of nitryl chloride using a chemical ionization mass spectrometer in
656 central London in the summer of 2012, and an investigation of the role of Cl atom oxidation,
657 *J. Geophys. Res.-Atmos.*, 120, 5638-5657, 2015.
- 658 Bedjanian, Y., Romanias, M. N., and El Zein, A.: Interaction of OH Radicals with Arizona
659 Test Dust: Uptake and Products, *J. Phys. Chem. A*, 117, 393-400, 2013.
- 660 Braesicke, P., Keeble, J., Yang, X., Stiller, G., Kellmann, S., Abraham, N. L., Archibald, A.,
661 Telford, P., and Pyle, J. A.: Circulation anomalies in the Southern Hemisphere and ozone
662 changes, *Atmos. Chem. Phys.*, 13, 10677-10688, 2013.
- 663 Burkholder, J. B., Sander, S. P., Abbatt, J. P. D., Barker, J. R., Huie, R. E., Kolb, C. E.,
664 Kurylo, M. J., Orkin, V. L., Wilmouth, D. M., and Wine, P. H.: Chemical Kinetics and
665 Photochemical Data for Use in Atmospheric Studies, Evaluation No. 18, JPL Publication 15-
666 10, Jet Propulsion Lab., Pasadena, CA, 2015.
- 667 Chen, H. H., Nanayakkara, C. E., and Grassian, V. H.: Titanium Dioxide Photocatalysis in
668 Atmospheric Chemistry, *Chem. Rev.*, 112, 5919-5948, 2012.
- 669 Chikazawa, M., Kanazawa, T., and Yamaguchi, T.: The Role of Adsorbed Water on
670 Adhesion Force of Powder Particles, *KONA*, 2, 54-61, 1984.
- 671 Crowley, J. N., Ammann, M., Cox, R. A., Hynes, R. G., Jenkin, M. E., Mellouki, A., Rossi,
672 M. J., Troe, J., and Wallington, T. J.: Evaluated Kinetic and Photochemical Data for
673 Atmospheric Chemistry: Volume V - Heterogeneous Reactions on Solid Substrates, *Atmos.*
674 *Chem. Phys.*, 10, 9059-9223, 2010.
- 675 Crutzen, P. J.: Albedo enhancement by stratospheric sulfur injections: A contribution to
676 resolve a policy dilemma?, *Clim. Change*, 77, 211-219, 2006.
- 677 Danilin, M. Y., Shia, R. L., Ko, M. K. W., Weisenstein, D. K., Sze, N. D., Lamb, J. J., Smith,
678 T. W., Lohn, P. D., and Prather, M. J.: Global stratospheric effects of the alumina emissions
679 by solid-fueled rocket motors, *J. Geophys. Res.-Atmos.*, 106, 12727-12738, 2001.
- 680 Davidson, J. A., Cantrell, C. A., Shetter, R. E., McDaniel, A. H., and Calvert, J. G.: Absolute
681 infrared absorption cross sections for ClONO₂ at 296 and 223 K, *J. Geophys. Res.-Atmos.*,
682 92, 10921-10925, 1987.
- 683 Dee, D. P., Uppala, S. M., Simmons, A. J., Berrisford, P., Poli, P., Kobayashi, S., Andrae, U.,
684 Balmaseda, M. A., Balsamo, G., Bauer, P., Bechtold, P., Beljaars, A. C. M., van de Berg, L.,
685 Bidlot, J., Bormann, N., Delsol, C., Dragani, R., Fuentes, M., Geer, A. J., Haimberger, L.,
686 Healy, S. B., Hersbach, H., Holm, E. V., Isaksen, L., Kallberg, P., Kohler, M., Matricardi,



- 687 M., McNally, A. P., Monge-Sanz, B. M., Morcrette, J. J., Park, B. K., Peubey, C., de Rosnay,
688 P., Tavolato, C., Thepaut, J. N., and Vitart, F.: The ERA-Interim reanalysis: configuration
689 and performance of the data assimilation system, *Q. J. R. Meteorol. Soc.*, 137, 553-597, 2011.
690 Deiber, G., George, C., Le Calvé, S., Schweitzer, F., and Mirabel, P.: Uptake study of
691 ClONO₂ and BrONO₂ by Halide containing droplets, *Atmos. Chem. Phys.*, 4, 1291-1299,
692 2004.
- 693 Dutton, E. G., and Christy, J. R.: Solar radiative forcing at selected locations and evidence for
694 global lower tropospheric cooling following the eruptions of El Chichón and Pinatubo,
695 *Geophys. Res. Lett.*, 19, 2313-2316, 1992.
- 696 Fahey, D. W., Eubank, C. S., Hubler, G., and Fehsenfeld, F. C.: A Calibrated Source of N₂O₅,
697 *Atmos. Environ.*, 19, 1883-1890, 1985.
- 698 Fahey, D. W., Kawa, S. R., Woodbridge, E. L., Tin, P., Wilson, J. C., Jonsson, H. H., Dye, J.
699 E., Baumgardner, D., Borrmann, S., Toohey, D. W., Avallone, L. M., Proffitt, M. H.,
700 Margitan, J., Loewenstein, M., Podolske, J. R., Salawitch, R. J., Wofsy, S. C., Ko, M. K. W.,
701 Anderson, D. E., Schoeberl, M. R., and Chan, K. R.: In situ measurement constraining the
702 role of sulfate aerosol in midlatitude ozone depletion, *Nature*, 363, 509-514, 1993.
- 703 Fernandez, M. A., Hynes, R. G., and Cox, R. A.: Kinetics of ClONO₂ reactive uptake on ice
704 surfaces at temperatures of the upper troposphere, *J. Phys. Chem. A*, 109, 9986-9996, 2005.
- 705 Ferraro, A. J., Highwood, E. J., and Charlton-Perez, A. J.: Stratospheric heating by potential
706 geoengineering aerosols, *Geophys. Res. Lett.*, 38, L24706, 10.1029/2011GL049761, 2011.
- 707 Finlayson-Pitts, B. J., Ezell, M. J., and Pitts, J. N.: Formation of Chemically Active Chlorine
708 Compounds by Reactions of Atmospheric NaCl Particles with Gaseous N₂O₅ and ClONO₂,
709 *Nature*, 337, 241-244, 1989.
- 710 George, C., Ammann, M., D'Anna, B., Donaldson, D. J., and Nizkorodov, S. A.:
711 Heterogeneous Photochemistry in the Atmosphere, *Chem. Rev.*, 115, 4218-4258, 2015.
- 712 Ginoux, P., Prospero, J. M., Gill, T. E., Hsu, N. C., and Zhao, M.: Global-scale Attribution of
713 Anthropogenic and Natural Dust Sources and Their Emission Rates Based on MODIS Deep
714 Blue Aerosol Products, *Rev. Geophys.*, 50, RG3005, doi: 3010.1029/2012RG000388, 2012.
- 715 Goodman, A. L., Bernard, E. T., and Grassian, V. H.: Spectroscopic Study of Nitric Acid and
716 Water Adsorption on Oxide Particles: Enhanced Nitric Acid Uptake Kinetics in the Presence
717 of Adsorbed Water, *J. Phys. Chem. A*, 105, 6443-6457, 2001.
- 718 Guo, S., Bluth, G. J. S., Rose, W. I., Watson, I. M., and Prata, A. J.: Re-evaluation of SO₂
719 release of the 15 June 1991 Pinatubo eruption using ultraviolet and infrared satellite sensors,
720 *Geochem. Geophys. Geosyst.*, 5, Q04001, doi: 04010.01029/02003GC000654, 2004.
- 721 Hanson, D. R., and Ravishankara, A. R.: The reaction probabilities of ClONO₂ and N₂O₅ on
722 polar stratospheric cloud materials, *J. Geophys. Res.-Atmos.*, 96, 5081-5090, 1991.
- 723 Hanson, D. R., and Ravishankara, A. R.: Reactive uptake of ClONO₂ onto sulfuric-acid due to
724 reaction with HCl and H₂O, *J. Phys. Chem.*, 98, 5728-5735, 1994.
- 725 Hanson, D. R., and Lovejoy, E. R.: The Reaction of ClONO₂ with Submicrometer Sulfuric-
726 Acid Aerosol, *Science*, 267, 1326-1328, 1995.
- 727 Hanson, D. R.: Reaction of ClONO₂ with H₂O and HCl in sulfuric acid and
728 HNO₃/H₂SO₄/H₂O mixtures, *J. Phys. Chem. A*, 102, 4794-4807, 1998.
- 729 Hinds, W. C.: Aerosol techniques: properties, behavior, and measurement of airborne
730 particles, John Wiley & Sons, Inc., New York, 1996.
- 731 Howard, C. J.: Kinetic Measurements Using Flow Tubes, *J. Phys. Chem.*, 83, 3-9, 1979.
- 732 Jackman, C. H., Considine, D. B., and Fleming, E. L.: A global modeling study of solid
733 rocket aluminum oxide emission effects on stratospheric ozone, *Geophys. Res. Lett.*, 25, 907-
734 910, 1998.



- 735 Jones, A. C., Haywood, J. M., and Jones, A.: Climatic impacts of stratospheric
736 geoengineering with sulfate, black carbon and titania injection, *Atmos. Chem. Phys.*, 16,
737 2843-2862, 2016.
- 738 Kebede, M. A., Scharko, N. K., Appelt, L. E., and Raff, J. D.: Formation of Nitrous Acid
739 during Ammonia Photooxidation on TiO₂ under Atmospherically Relevant Conditions, *J.*
740 *Phys. Chem. Lett.*, 4, 2618-2623, 2013.
- 741 Keeble, J., Braesicke, P., Abraham, N. L., Roscoe, H. K., and Pyle, J. A.: The impact of polar
742 stratospheric ozone loss on Southern Hemisphere stratospheric circulation and climate,
743 *Atmos. Chem. Phys.*, 14, 13705-13717, 2014.
- 744 Kravitz, B., Robock, A., Forster, P. M., Haywood, J. M., Lawrence, M. G., and Schmidt, H.:
745 An overview of the Geoengineering Model Intercomparison Project (GeoMIP), *J. Geophys.*
746 *Res.-Atmos.*, 118, 13103-13107, 2013.
- 747 Lawler, M. J., Sander, R., Carpenter, L. J., Lee, J. D., von Glasow, R., Sommariva, R., and
748 Saltzman, E. S.: HOCl and Cl₂ observations in marine air, *Atmos. Chem. Phys.*, 11, 7617-
749 7628, 2011.
- 750 Lee, S. H., Leard, D. C., Zhang, R. Y., Molina, L. T., and Molina, M. J.: The HCl+ClONO₂
751 reaction rate on various water ice surfaces, *Chem. Phys. Lett.*, 315, 7-11, 1999.
- 752 Liao, J., Huey, L. G., Liu, Z., Tanner, D. J., Cantrell, C. A., Orlando, J. J., Flocke, F. M.,
753 Shepson, P. B., Weinheimer, A. J., Hall, S. R., Ullmann, K., Beine, H. J., Wang, Y., Ingall, E.
754 D., Stephens, C. R., Hornbrook, R. S., Apel, E. C., Riemer, D., Fried, A., Mauldin III, R. L.,
755 Smith, J. N., Staebler, R. M., Neuman, J. A., and Nowak, J. B.: High levels of molecular
756 chlorine in the Arctic atmosphere, *Nature Geosci.*, 7, 91-94, 2014.
- 757 McCormick, M. P., Thomason, L. W., and Trepte, C. R.: Atmospheric effects of the Mt
758 Pinatubo eruption, *Nature*, 373, 399-404, 1995.
- 759 Molina, L. T., Spencer, J. E., and Molina, M. J.: The rate constant for the reaction of O(³P)
760 atoms with ClONO₂, *Chem. Phys. Lett.*, 45, 158-162, 1977.
- 761 Molina, M. J., Molina, L. T., and Kolb, C. E.: Gas-phase and heterogeneous chemical
762 kinetics of the troposphere and stratosphere, *Annu. Rev. Phys. Chem.*, 47, 327-367, 1996.
- 763 Molina, M. J., Molina, L. T., Zhang, R. Y., Meads, R. F., and Spencer, D. D.: The reaction of
764 ClONO₂ with HCl on aluminum oxide, *Geophys. Res. Lett.*, 24, 1619-1622, 1997.
- 765 Morgenstern, O., Braesicke, P., O'Connor, F. M., Bushell, A. C., Johnson, C. E., Osprey, S.
766 M., and Pyle, J. A.: Evaluation of the new UKCA climate-composition model – Part 1: The
767 stratosphere, *Geosci. Model Dev.*, 2, 43-57, 2009.
- 768 O'Connor, F. M., Johnson, C. E., Morgenstern, O., Abraham, N. L., Braesicke, P., Dalvi, M.,
769 Folberth, G. A., Sanderson, M. G., Telford, P. J., Voulgarakis, A., Young, P. J., Zeng, G.,
770 Collins, W. J., and Pyle, J. A.: Evaluation of the new UKCA climate-composition model –
771 Part 2: The Troposphere, *Geosci. Model Dev.*, 7, 41-91, 2014.
- 772 Osthoff, H. D., Roberts, J. M., Ravishankara, A. R., Williams, E. J., Lerner, B. M.,
773 Sommariva, R., Bates, T. S., Coffman, D., Quinn, P. K., Dibb, J. E., Stark, H., Burkholder, J.
774 B., Talukdar, R. K., Meagher, J., Fehsenfeld, F. C., and Brown, S. S.: High levels of nitryl
775 chloride in the polluted subtropical marine boundary layer, *Nature Geosci.*, 1, 324-328, 2008.
- 776 Phillips, G. J., Tang, M. J., Thieser, J., Brickwedde, B., Schuster, G., Bohn, B., Lelieveld, J.,
777 and Crowley, J. N.: Significant concentrations of nitryl chloride observed in rural continental
778 Europe associated with the influence of sea salt chloride and anthropogenic emissions,
779 *Geophys. Res. Lett.*, 39, L10811, 10.1029/2012gl051912, 2012.
- 780 Pope, F. D., Braesicke, P., Grainger, R. G., Kalberer, M., Watson, I. M., Davidson, P. J., and
781 Cox, R. A.: Stratospheric aerosol particles and solar-radiation management, *Nature Clim.*
782 *Change*, 2, 713-719, 2012.
- 783 Renard, J. J., and Bolker, H. I.: The chemistry of chlorine monoxide (dichlorine monoxide),
784 *Chem. Rev.*, 76, 487-508, 1976.



- 785 Riedel, T. P., Bertram, T. H., Crisp, T. A., Williams, E. J., Lerner, B. M., Vlasenko, A., Li,
786 S.-M., Gilman, J., de Gouw, J., Bon, D. M., Wagner, N. L., Brown, S. S., and Thornton, J. A.:
787 Nitryl Chloride and Molecular Chlorine in the Coastal Marine Boundary Layer, *Environ. Sci.*
788 *Technol.*, 46, 10463-10470, 2012.
- 789 Robinson, G. N., Worsnop, D. R., Jayne, J. T., Kolb, C. E., and Davidovits, P.:
790 Heterogeneous uptake of ClONO₂ and N₂O₅ by sulfuric acid solutions, *J. Geophys. Res.-*
791 *Atmos.*, 102, 3583-3601, 1997.
- 792 Romanias, M. N., El Zein, A., and Bedjanian, Y.: Heterogeneous Interaction of H₂O₂ with
793 TiO₂ Surface under Dark and UV Light Irradiation Conditions, *J. Phys. Chem. A*, 116, 8191-
794 8200, 2012.
- 795 Rouviere, A., Sosedova, Y., and Ammann, M.: Uptake of Ozone to Deliquesced KI and
796 Mixed KI/NaCl Aerosol Particles, *J. Phys. Chem. A*, 114, 7085-7093, 2010.
- 797 Schack, C. J., and Lindahl, C. B.: On the synthesis of chlorine monoxide, *Inorg. Nucl.*
798 *Chem. Lett.*, 3, 387-389, 1967.
- 799 Seisel, S., Borensen, C., Vogt, R., and Zellner, R.: Kinetics and Mechanism of the Uptake of
800 N₂O₅ on Mineral Dust at 298 K, *Atmos. Chem. Phys.*, 5, 3423-3432, 2005.
- 801 Shang, J., Li, J., and Zhu, T.: Heterogeneous Reaction of SO₂ on TiO₂ Particles, *Sci. China*
802 *Chem.*, 53, 2637-2643, 2010.
- 803 Shepherd, J.: *Geoengineering the climate: science, governance and uncertainty*, The Royal
804 Society, London, UK, 2009.
- 805 Shi, Q., Jayne, J. T., Kolb, C. E., Worsnop, D. R., and Davidovits, P.: Kinetic model for
806 reaction of ClONO₂ with H₂O and HCl and HOCl with HCl in sulfuric acid solutions, *J.*
807 *Geophys. Res.-Atmos.*, 106, 24259-24274, 2001.
- 808 Simpson, W. R., Brown, S. S., Saiz-Lopez, A., Thornton, J. A., and Glasow, R. v.:
809 Tropospheric Halogen Chemistry: Sources, Cycling, and Impacts, *Chem. Rev.*, 115, 4035-
810 4062, 2015.
- 811 Solomon, S.: Stratospheric ozone depletion: A review of concepts and history, *Rev.*
812 *Geophys.*, 37, 275-316, 1999.
- 813 SPARC: Assessment of Stratospheric Aerosol Properties (SPARCR Report No. 4), 2006.
- 814 Spicer, C. W., Chapman, E. G., Finlayson-Pitts, B. J., Plastringe, R. A., Hubbe, J. M., Fast, J.
815 D., and Berkowitz, C. M.: Unexpectedly high concentrations of molecular chlorine in coastal
816 air, *Nature*, 394, 353-356, 1998.
- 817 Stull, D. R.: Vapor Pressure of Pure Substances. *Organic and Inorganic Compounds*, Ind.
818 *Eng. Chem.*, 39, 517-540, 1947.
- 819 Tang, M. J., Thieser, J., Schuster, G., and Crowley, J. N.: Kinetics and Mechanism of the
820 Heterogeneous Reaction of N₂O₅ with Mineral Dust Particles, *Phys. Chem. Chem. Phys.*, 14,
821 8551-8561, 2012.
- 822 Tang, M. J., Camp, J. C. J., Rkiouak, L., McGregor, J., Watson, I. M., Cox, R. A., Kalberer,
823 M., Ward, A. D., and Pope, F. D.: Heterogeneous Interaction of SiO₂ with N₂O₅: Aerosol
824 Flow Tube and Single Particle Optical Levitation-Raman Spectroscopy Studies, *J. Phys.*
825 *Chem. A*, 118, 8817-8827, 2014a.
- 826 Tang, M. J., Cox, R. A., and Kalberer, M.: Compilation and Evaluation of Gas Phase
827 Diffusion Coefficients of Reactive Trace Gases in the Atmosphere: Volume 1. Inorganic
828 Compounds, *Atmos. Chem. Phys.*, 14, 9233-9247, 2014b.
- 829 Tang, M. J., Schuster, G., and Crowley, J. N.: Heterogeneous Reaction of N₂O₅ with Illite
830 and Arizona Test Dust Particles, *Atmos. Chem. Phys.*, 14, 245-254, 2014c.
- 831 Tang, M. J., Telford, P. J., Pope, F. D., Rkiouak, L., Abraham, N. L., Archibald, A. T.,
832 Braesicke, P., Pyle, J. A., McGregor, J., Watson, I. M., Cox, R. A., and Kalberer, M.:
833 Heterogeneous reaction of N₂O₅ with airborne TiO₂ particles and its implication for
834 stratospheric particle injection, *Atmos. Chem. Phys.*, 14, 6035-6048, 2014d.



- 835 Tang, M. J., Cziczo, D. J., and Grassian, V. H.: Interactions of Water with Mineral Dust
836 Aerosol: Water Adsorption, Hygroscopicity, Cloud Condensation and Ice Nucleation, *Chem.*
837 *Rev.*, 116, 4205–4259, 2016.
- 838 Telford, P., Braesicke, P., Morgenstern, O., and Pyle, J.: Reassessment of causes of ozone
839 column variability following the eruption of Mount Pinatubo using a nudged CCM, *Atmos.*
840 *Chem. Phys.*, 9, 4251-4260, 2009.
- 841 Telford, P. J., Braesicke, P., Morgenstern, O., and Pyle, J. A.: Technical Note: Description
842 and assessment of a nudged version of the new dynamics Unified Model, *Atmos. Chem.*
843 *Phys.*, 8, 1701-1712, 2008.
- 844 Textor, C., Schulz, M., Guibert, S., Kinne, S., Balkanski, Y., Bauer, S., Berntsen, T., Berglen,
845 T., Boucher, O., Chin, M., Dentener, F., Diehl, T., Easter, R., Feichter, H., Fillmore, D.,
846 Ghan, S., Ginoux, P., Gong, S., Grini, A., Hendricks, J., Horowitz, L., Huang, P., Isaksen, I.,
847 Iversen, I., Kloster, S., Koch, D., Kirkevåg, A., Kristjansson, J. E., Krol, M., Lauer, A.,
848 Lamarque, J. F., Liu, X., Montanaro, V., Myhre, G., Penner, J., Pitari, G., Reddy, S., Seland,
849 Ø., Stier, P., Takemura, T., and Tie, X.: Analysis and Quantification of the Diversities of
850 Aerosol Life Cycles within AeroCom, *Atmos. Chem. Phys.*, 6, 1777-1813, 2006.
- 851 Thornton, J. A., Kercher, J. P., Riedel, T. P., Wagner, N. L., Cozic, J., Holloway, J., S., Dube,
852 W. P., Wolfe, G. M., Quinn, P. K., Middlebrook, A. M., Alexander, B., and Brown, S. S.: A
853 large atomic chlorine source inferred from mid-continental reactive nitrogen chemistry,
854 *Nature*, 464, 271-174, 2010.
- 855 Tilmes, S., Muller, R., and Salawitch, R.: The sensitivity of polar ozone depletion to
856 proposed geoengineering schemes, *Science*, 320, 1201-1204, 2008.
- 857 Tilmes, S., Mills, M. J., Niemeier, U., Schmidt, H., Robock, A., Kravitz, B., Lamarque, J. F.,
858 Pitari, G., and English, J. M.: A new Geoengineering Model Intercomparison Project
859 (GeoMIP) experiment designed for climate and chemistry models, *Geosci. Model Dev.*, 8,
860 43-49, 2015.
- 861 Wagner, C., Hanisch, F., Holmes, N., de Coninck, H., Schuster, G., and Crowley, J. N.: The
862 interaction of N_2O_5 with mineral dust: aerosol flow tube and Knudsen reactor studies, *Atmos.*
863 *Chem. Phys.*, 8, 91-109, 2008.
- 864 Wang, T., Tham, Y. J., Xue, L., Li, Q., Zha, Q., Wang, Z., Poon, S. C. N., Dubé, W. P.,
865 Blake, D. R., Louie, P. K. K., Luk, C. W. Y., Tsui, W., and Brown, S. S.: Observations of
866 nitryl chloride and modeling its source and effect on ozone in the planetary boundary layer of
867 southern China, *J. Geophys. Res.-Atmos.*, 121, 2476-2489, 2016.
- 868 Weisenstein, D. K., Keith, D. W., and Dykema, J. A.: Solar geoengineering using solid
869 aerosol in the stratosphere, *Atmos. Chem. Phys.*, 15, 11835-11859, 2015.
- 870 Wilson, J. C., Jonsson, H. H., Brock, C. A., Toohey, D. W., Avallone, L. M., Baumgardner,
871 D., Dye, J. E., Poole, L. R., Woods, D. C., Decoursey, R. J., Osborn, M., Pitts, M. C., Kelly,
872 K. K., Chan, K. R., Ferry, G. V., Loewenstein, M., Podolske, J. R., and Weaver, A.: In-situ
873 observations of aerosol and chlorine monoxide after the 1991 eruption of Mount-Pinatubo:
874 effect of reactions on sulfate aerosol, *Science*, 261, 1140-1143, 1993.
- 875 Wu, L.-Y., Tong, S.-R., Hou, S.-Q., and Ge, M.-F.: Influence of Temperature on the
876 Heterogeneous Reaction of Formic Acid on $\alpha\text{-Al}_2\text{O}_3$, *J. Phys. Chem. A*, 116, 10390-10396,
877 2012.
- 878 Zhang, R. Y., Jayne, J. T., and Molina, M. J.: Heterogeneous interacyions of ClONO_2 and
879 HCl with sulfuric acid tetrahydrate: implications for the stratosphere, *J. Phys. Chem.*, 98,
880 867-874, 1994.
- 881
882

883 **Tables& Figures**884 **Table 1.** Loss rates and uptake coefficients of ClONO₂ onto the inner wall of the Pyrex tube at

885 different relative humidities (RH).

RH (%)	$k_w (\times 10^{-2} \text{ s}^{-1})$	$\gamma (\times 10^{-6})$
0	3.6±0.2	5.1±0.3
	2.9±0.4	3.9±0.6
6	4.1±0.1	6.2±0.1
	3.7±0.7	5.4±1.0
12	4.1±0.3	6.2±0.5
17	6.9±0.3	13±0.6
	6.4±0.2	11±0.4
24	8.1±0.8	16±2.0
	8.2±0.3	17±0.7

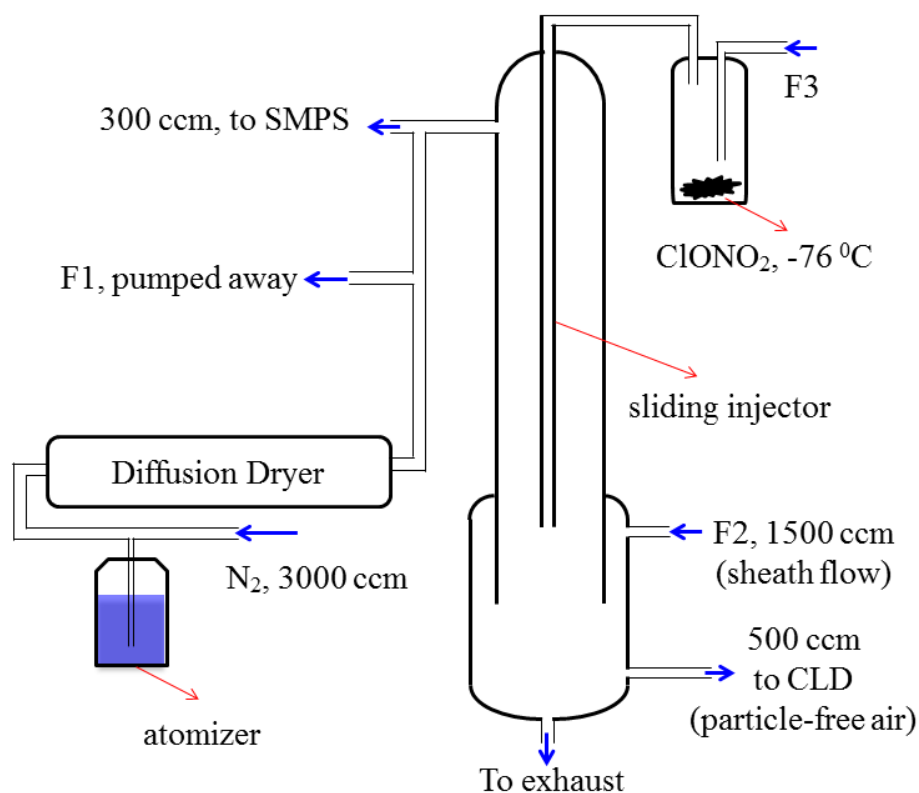
886



887 **Table 2.** Uptake coefficients of ClONO₂ onto SiO₂ and TiO₂ aerosol particles at different
 888 relative humidities (RH). *k_a*: loss rate of ClONO₂ onto aerosol particle surface; *S_a*: aerosol
 889 surface area concentration; $\gamma(\text{ClONO}_2)$: uptake coefficients of ClONO₂.

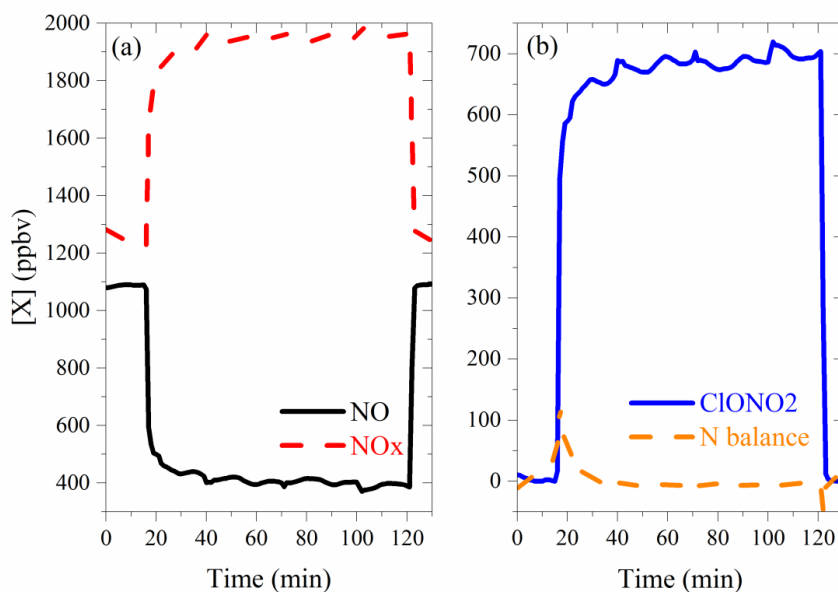
Particle	RH (%)	<i>k_a</i> ($\times 10^{-3}$ s)	<i>S_a</i> ($\times 10^{-3}$ cm ² cm ⁻³)	$\gamma(\text{ClONO}_2)$ ($\times 10^{-4}$)
SiO ₂	7±1	4.1±2.5	2.80±0.02	2.3±1.4
	7±1	3.4±3.2	2.78±0.05	1.9±1.8
	17±2	<5.1 ^a	1.08±0.08	<7.5 ^a
	17±2	<5.4 ^a	1.28±0.07	<6.7 ^a
	17±2	<7.3 ^a	1.78±0.09	<6.5 ^a
	17±2	6.5±4.2	2.08±0.06	4.9±3.2
	35±4	6.3±3.1	2.34±0.08	4.2±2.1
	35±4	13.1±4.7	2.91±0.09	7.1±2.6
	35±4	9.0±7.3	2.86±0.10	4.8±3.9
	59±3	11.6±3.5	2.88±0.06	6.4±1.9
TiO ₂	7±1	7.0±1.4	1.09±0.12	10.1±2.0
	7±1	6.2±2.3	0.73±0.05	13.7±5.0
	33±3	17.9±5.6	2.23±0.03	12.7±3.9
	33±3	14.5±1.4	1.93±0.03	11.9±1.1

890 a: estimated upper limits.



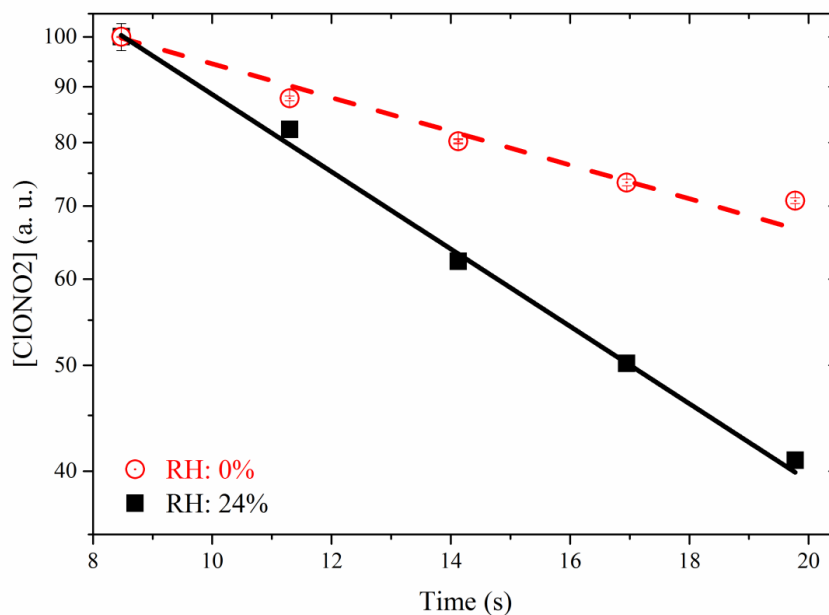
891

892 **Figure 1.** Schematic diagram of the aerosol flow tube used in this study. SMPS: Scanning
893 Mobility Particle Sizer; CLD: Chemiluminescence detector, used to measure the ClONO_2
894 concentration (measured as the change in NO concentration). All the flows (except the flow
895 applied to the atomizer) were controlled by mass flow controllers. Flow details are provided in
896 text.



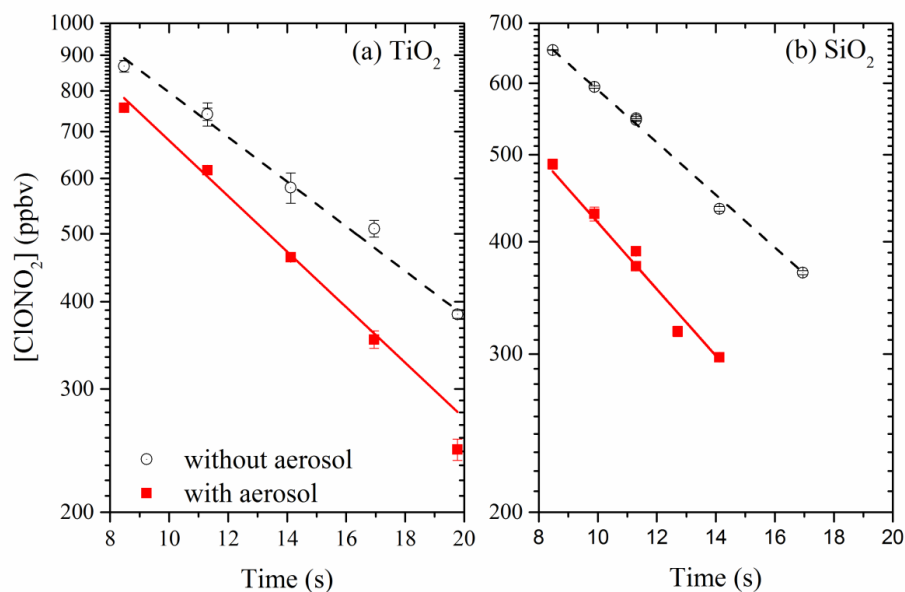
897

898 **Figure 2.** Response of measured NO and NOx mixing ratios to the introduction of ClONO₂
899 into the flow tube (left panel). The corresponding calculated ClONO₂ mixing ratio and nitrogen
900 balance are also shown (right panel).



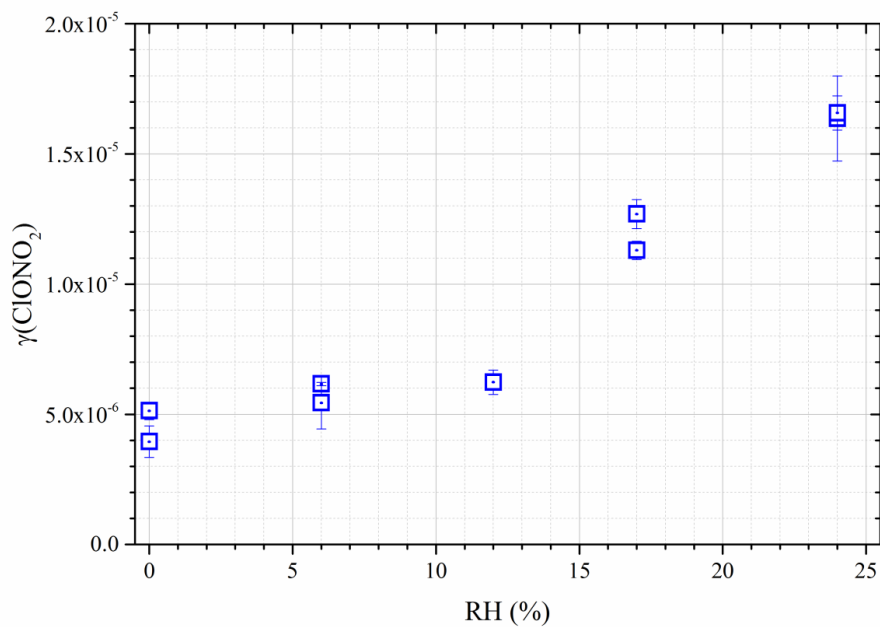
901

902 **Figure 3.** Decays of ClONO₂ in the flow tube due to its loss onto the Pyrex glass (circles: 0%
903 RH; squares: 24% RH). Measured ClONO₂ mixing ratios were normalized to that at 8.5 s (when
904 the injector was at 30 cm). Typical ClONO₂ mixing ratios in the flow tube are a few hundred
905 ppbv (see Figure 2).



906

907 **Figure 4.** Decays of ClONO₂ in the aerosol flow tube without (open circles) and with (solid
908 squares) aerosol particles in the aerosol flow tube under different experimental conditions. (a)
909 TiO₂ with a surface area concentration of $2.3 \times 10^{-3} \text{ cm}^2 \text{ cm}^{-3}$ at 33% RH; (b) SiO₂ with a surface
910 area concentration of $2.9 \times 10^{-3} \text{ cm}^2 \text{ cm}^{-3}$ at 39% RH.

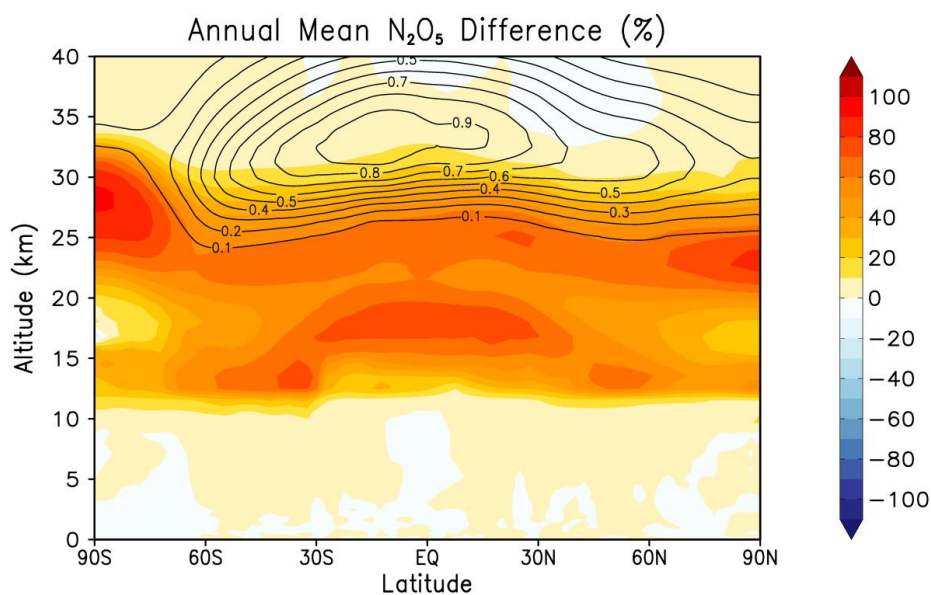


911

912 **Figure 5.** Dependence of $\gamma(\text{ClONO}_2)$ on RH for Pyrex glass.



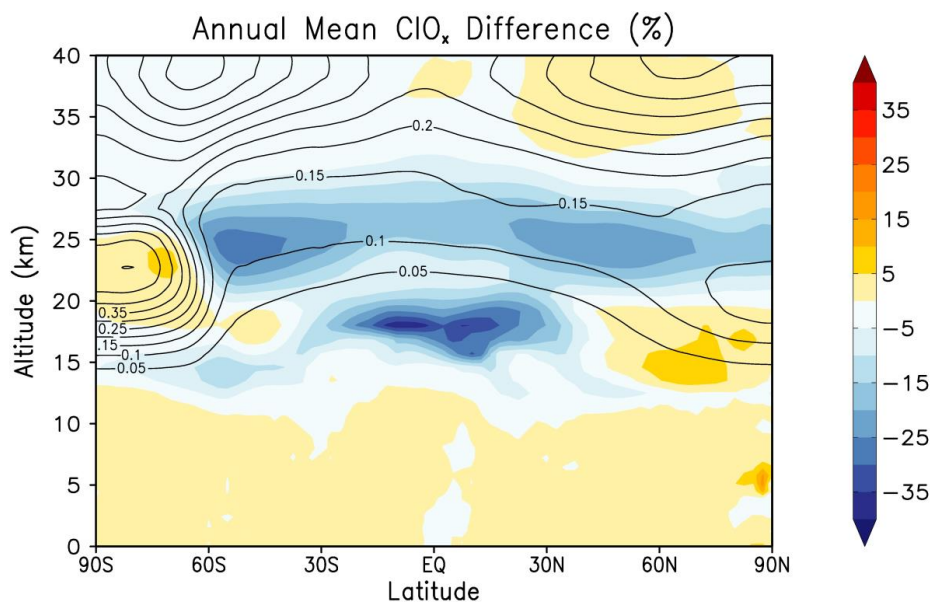
913



914
915 **Figure 6.** Simulated annual mean, zonal mean N_2O_5 percentage differences between TiO_2
916 injection (S3) and the Mt Pinatubo eruption (S2). Black contour lines show N_2O_5 mixing ratios
917 from the Mt Pinatubo simulation (S2) in ppb.

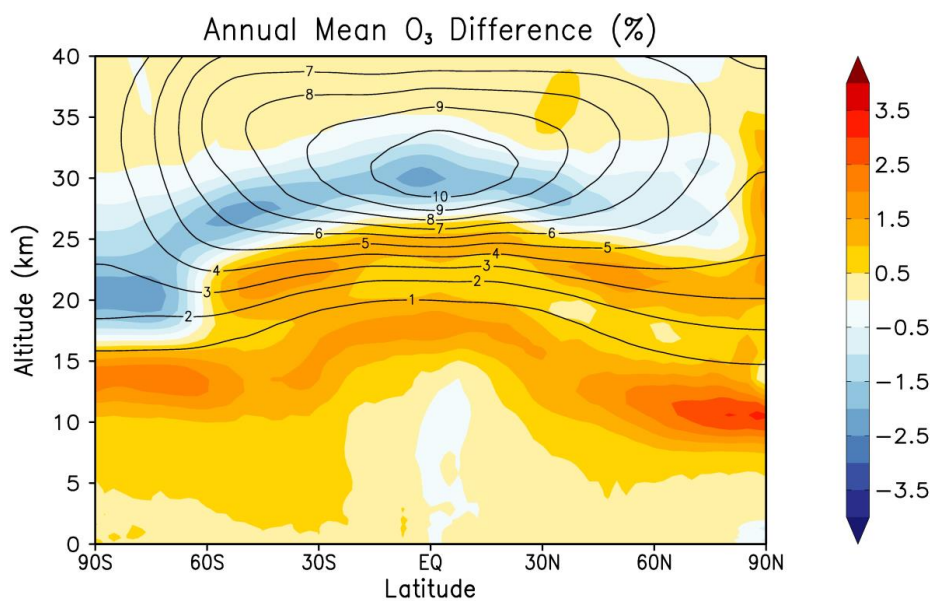


918



919

920 **Figure 7.** Simulated annual mean, zonal mean ClO_x percentage differences between TiO₂
921 injection (S3) and the Mt Pinatubo eruption (S2). Black contour lines show ClO_x mixing ratios
922 from the Mt Pinatubo simulation (S2) in ppb.



923

924 **Figure 8.** Simulated annual mean, zonal mean O₃ percentage differences between TiO₂
925 injection (S3) and the Mt Pinatubo eruption (S2). Black contour lines show ClO_x mixing ratios
926 from the Mt Pinatubo simulation (S2) in ppmv.